

EDIpack: A parallel exact diagonalization package for quantum impurity problems

A. Amaricci^{a,*}, L. Crippa^{b,c}, A. Scazzola^b, F. Petocchi^d, G. Mazza^e, L. de Medici^f,
M. Capone^b

^a*CNR-IOM, Istituto Officina dei Materiali, Consiglio Nazionale delle Ricerche, Via Bonomea 265, 34136 Trieste, Italy*

^b*Scuola Internazionale Superiore di Studi Avanzati (SISSA), Via Bonomea 265, 34136 Trieste, Italy*

^c*Institut für Theoretische Physik und Astrophysik and Würzburg-Dresden Cluster of Excellence ct.qmat, Universität Würzburg, 97074 Würzburg, Germany*

^d*Department of Physics, University of Fribourg, 1700 Fribourg, Switzerland*

^e*Department of Quantum Matter Physics, University of Geneva, Quai Ernest-Ansermet 24, 1211 Geneva, Switzerland*

^f*LPEM, ESPCI Paris, PSL Research University, CNRS, Sorbonne Université, 75005 Paris, France*

Abstract

We present EDIpack, an exact diagonalization package to solve generic quantum impurity problems. The algorithm, based on a generalization of the look-up method introduced in Ref. 1, enables a massively parallel execution of the matrix-vector linear operations required by Lanczos and Arnoldi algorithms. We show that a suitable Fock basis organization is crucial to optimize the inter-processors communication in distributed memory setup and, thus, to reach sub-linear scaling in sufficiently large systems. We discuss the algorithm in details, indicating how to deal with multiple-orbitals and electron-phonon coupling. Finally, we detail the download, installation and functioning of this package.

Keywords: Exact diagonalization, Quantum Impurity models, Strongly correlated electrons, Dynamical Mean-Field Theory

PROGRAM SUMMARY

Program Title: EDIpack

Licensing provisions: GNU General Public License (GPL v3)

Programming language: Fortran, Python

Classification: 6.5, 7.4, 20

Required dependencies: CMake ($\geq 3.0.0$), Scifortran, MPI

Nature of problem: Solution of multi-orbital quantum impurity systems are at zero or low temperatures are considerably difficult to determine. Effective solution of lattice models of strongly correlated electrons.

*Corresponding author.

E-mail address: amaricci@sissa.it

Solution method: Use parallel exact diagonalization algorithm exploiting different conserved quantum numbers and product structure of the Fock space to compute dynamical correlation functions.

1. Introduction

The quantum impurity models² play a primary role in the effective description of the local properties of strongly correlated electron systems³. Indeed, the reduction of complicated lattice models of correlated electrons to effective impurity systems within dynamical mean-field theory³⁻⁶ (DMFT) or variational cluster approximations⁷⁻¹⁰ boosted our understanding of correlated materials properties. This scientific advance was partially supported by the development of many numerical methods to solve impurity problems within different approximation schemes^{11,12}, such as the continuous-time quantum Monte Carlo approaches¹³⁻¹⁷ the numerical renormalization group¹⁸⁻²⁰ or the density-matrix renormalization group²¹⁻²⁵. Among these state-of-the-art methods, the Exact Diagonalization (ED) impurity solver²⁶⁻³¹ plays a relevant role. The ED method relies on the construction of all or part of the spectrum of a finite quantum system by solving the associated eigenvalue problem, giving access to zero or low temperature properties as well as exact calculation of one-particle correlation functions on the entire complex plane. This method is not limited to quantum impurity models and the ideas presented in this manuscript can be applied also to a wide range of finite-size quantum systems^{32,33}.

In the context of DMFT it has been shown that quantum impurity models with a small Hilbert space already provide accurate results. However, the required size rapidly increases if we consider multi-orbital problems or we include the coupling with phonons. As well, larger systems are also required to resolve small energy or temperature scales. The exponential growth of the Hilbert space is however the bottleneck of ED calculations. In order to overcome such limitations it is mandatory to profit of the blossoming of multi-threaded calculations made available in high-performance computers. In this respect, it is crucial to progress the development of ED algorithm for impurity problems in the direction of parallel computing³⁴⁻³⁶. Yet, the parallel formulation of the ED algorithms^{27,34,36,37} can be tremendously more complicated with respect to other methods, e.g. Quantum Monte Carlo, due to the handling of the required inter-processor communications.

In this work we present a detailed implementation of a parallel ED algorithm to solve generic quantum impurity problems, including multi-orbital character as well as electron-phonon coupling. This parallel algorithm can be easily adapted to other electronic systems on a lattice. We show that under very general conditions a nearly linear scaling of the algorithm with the number of processors can be achieved, making it possible to solve large systems in a relatively short time and with a moderate distributed memory use. The key step of the ED algorithm is the organization of the Hilbert space and the construction of a suitable basis of electronic configurations^{1,37}. In such a basis the Hamiltonian is represented by an exponentially large matrix which makes it impossible to store it, let alone to diagonalize it. The Hamiltonian has however a sparse nature, i.e. a largely reduced number of finite entries with respect to the total. This allows to reduce the memory footprint and to exploit powerful

algorithms designed to obtain the sparse matrices spectra^{37–41}. Such methods generally rely on linear operations, like the matrix-vector products, which in turn constitute the largest portion of the computational time. A generic and efficient optimization of these operations is then critical to reduce the computational effort. Here we discuss how to organize the Hilbert space basis in presence of multiple conserved quantum numbers and how to profit of this within matrix-vector operations so to avoid inter-processor communication congestion and unlock favorable scaling.

The rest of this work is organized as follows: In Sec. 2 we introduce the generic quantum impurity problem and discuss the relevant aspects of the ED method for a generic multi-orbital implementation. In Sec. 3 we discuss the parallel algorithms designed to accelerate the execution of the matrix-vector products, at the heart of the ED method. In Sec. 4 we discuss the extension the ED algorithm to the case of electron-phonon coupling, including the modifications imposed to the distributed parallelization. Next, in Sec. 5 we discuss in details the scaling properties of this algorithm and their dependence on the number of orbitals and electron-phonon coupling. In Sec. 6 we give an overview of the library structure and discuss the essential aspects of the code implementation. Finally, in Sec. 7 we briefly describe the installation and basic use of the program.

2. Exact Diagonalization

2.1. The multi-orbital quantum impurity problem

We consider a system of N_s electronic levels. A portion N_α of them, i.e. the impurity levels, interact via a local repulsion, while the remaining $N_s - N_\alpha$, i.e. the *bath* levels, are non-interacting. In a typical setup the impurity levels are independently coupled to a set of N_b electronic levels, so that the total number is $N_s = N_\alpha(N_b + 1)$. Other choices of the bath topology correspond to different counting of the total levels. The Hamiltonian of the electronic system we consider has the form:

$$\begin{aligned}
\hat{H}^e &= \hat{H}^0 + \hat{H}^{int} \\
\hat{H}^0 &= \sum_{\alpha\beta\sigma} H_{\alpha\beta\sigma}^{loc} d_{\alpha\sigma}^+ d_{\beta\sigma} + \\
&\quad \sum_{\nu\alpha\beta\sigma} h_{\alpha\beta\sigma}^\nu a_{\nu\alpha\sigma}^+ a_{\nu\beta\sigma} + \sum_{\nu\alpha\sigma} V_{\alpha\sigma}^\nu d_{\alpha\sigma}^+ a_{\nu\alpha\sigma} + H.c. \\
\hat{H}^{int} &= U \sum_{\alpha} n_{\alpha\uparrow} n_{\alpha\downarrow} + U' \sum_{\alpha\neq\beta} n_{\alpha\uparrow} n_{\beta\downarrow} + (U' - J) \sum_{\alpha<\beta,\sigma} n_{\alpha\sigma} n_{\beta\sigma} - \\
&\quad J \sum_{\alpha\neq\beta} d_{\alpha\uparrow}^+ d_{\alpha\downarrow} d_{\beta\downarrow}^+ d_{\beta\uparrow} + J \sum_{\alpha\neq\beta} d_{\alpha\uparrow}^+ d_{\alpha\downarrow}^+ d_{\beta\downarrow} d_{\beta\uparrow}
\end{aligned} \tag{1}$$

where $a_{\alpha\sigma}$, $d_{\alpha\sigma}$ ($a_{\alpha\sigma}^+$, $d_{\alpha\sigma}^+$) are, respectively, the destruction (creation) operators for the bath and impurity electrons with orbital α and spin σ , $n_{\alpha\sigma} = d_{\alpha\sigma}^+ d_{\alpha\sigma}$. The term $H_{\alpha\beta\sigma}^{loc}$ is the non-interacting part of the impurity Hamiltonian, $h_{\alpha\beta\sigma}^\nu$ and $V_{\alpha\sigma}^\nu$ are, respectively, the local Hamiltonian and the impurity hybridization of the ν -th bath level. Finally, \hat{H}^{int} is the local

multi-orbital Kanamori interaction⁴². U is the local Coulomb interaction strength, J is the Hund's coupling and $U' = U - 2J$ ⁴². The first three terms represent the density-density part of the interaction, while the remaining two in the second line are, respectively, the spin-exchange and pair-hopping terms.

2.2. The Fock space and conserved quantum numbers

A system of N_s electrons is associated to a Fock space of the form $\mathcal{F}_e = \bigoplus_{n=0}^{N_s} S_- \mathcal{H}_e^{\otimes n}$, where $\mathcal{H}_e = \{|0\rangle, |\uparrow\rangle, |\downarrow\rangle, |\uparrow\downarrow\rangle\}$ is the local Hilbert space of the electrons on a single level, S_- is the anti-symmetrization operator, \bigoplus is the direct sum and \bigotimes the tensor product. The total dimension of the Fock space \mathcal{F}_e is $\dim(\mathcal{H}_e)^{N_s} = 4^{N_s} = 2^{2N_s}$.

The solution of the eigenvalue problem for H_e is simplified by taking into account the existence of conserved quantities. The Hamiltonian (1) conserves the total charge \hat{N} and the spin component \hat{S}_z , as far as we assume that no terms breaking the particle number or spin conservation are present, e.g. local spin-orbital coupling, in-plane magnetic field, superconducting order, etc. The conservation of \hat{N} and \hat{S}_z can be conveniently re-expressed in terms of conserved number of electrons with spin \uparrow and \downarrow , i.e. $\hat{N}_\uparrow, \hat{N}_\downarrow$. Moreover, if the terms H^{loc} and h are diagonal, the number of electrons with spin \uparrow and \downarrow is conserved *per orbital*, i.e. $\hat{N}_\uparrow^\alpha, \hat{N}_\downarrow^\alpha$, where $\alpha = 1, \dots, N_\alpha$.

In order to formally unify the treatment of these two cases we introduce some convenient parameters, namely the number of conserved operators per spin $N_{ud} = 1$ (N_α) and the number of bits $N_{bit} = N_s$ (N_s/N_α) for conserved total (orbital resolved) number of electrons with spin \uparrow and \downarrow . In the rest of this work we will indicate the set of conserved quantum numbers (QN)s with the tuple $[\vec{N}_\uparrow, \vec{N}_\downarrow]$, where ($\sigma = \uparrow, \downarrow$):

$$\vec{N}_\sigma = \begin{cases} N_{1\sigma} \equiv N_\sigma, & \text{if } N_{ud} = 1 \\ [N_{1\sigma}, \dots, N_{N_\alpha\sigma}], & \text{if } N_{ud} = N_\alpha \end{cases} \quad (2)$$

In presence of a set of conserved QNs, the Fock space decomposes into a number of sub-spaces of reduced dimensions, each corresponding to a given value of the QNs tuple. We indicate each sub-space with the term *sector* and the symbol $\mathcal{S}[\vec{N}_\uparrow, \vec{N}_\downarrow]$, or just \mathcal{S} where no confusion arises. The dimension of each sector is given by the number of ways we can arrange $N_{\alpha\sigma}$ elements into N_{bit} positions, i.e.:

$$\begin{aligned} \dim\left(\mathcal{S}[\vec{N}_\uparrow, \vec{N}_\downarrow]\right) &= \prod_{\alpha=1}^{N_{ud}} \binom{N_{bit}}{N_{\alpha\uparrow}} \prod_{\alpha=1}^{N_{ud}} \binom{N_{bit}}{N_{\alpha\downarrow}} \\ &\equiv \prod_{\alpha=1}^{N_{ud}} D_{\alpha\uparrow} \prod_{\alpha=1}^{N_{ud}} D_{\alpha\downarrow} \stackrel{\text{def}}{=} D_\uparrow D_\downarrow \equiv D_{\mathcal{S}} \end{aligned} \quad (3)$$

where we introduced the symbols D_σ and $D_{\alpha\sigma}$ to indicate, respectively, the dimension of total and orbital spin-subspace associated to the given set of QNs. Note that $D_\sigma \equiv D_{1,\sigma}$ for $N_{ud} = 1$.

2.3. The basis states

A natural representation of the basis states for the Fock space \mathcal{F}_e is obtained in the occupation number formalism of second quantization. The *Fock basis* for a finite system of N_s electrons is composed of states of the form $|\vec{n}\rangle = |n_{1\uparrow}, \dots, n_{N_s\uparrow}, n_{1\downarrow}, \dots, n_{N_s\downarrow}\rangle$, where each element $n_{a\sigma} = 0, 1$ describes the absence or the presence of an electron with spin σ at the level a . In conjunction to the basis states, we introduce the non-Hermitian, anti-commuting, annihilation and creation operators $c_{a\sigma}$ and $c_{a\sigma}^+$, respectively. These operators act on the states $|\vec{n}\rangle$ as:

$$c_{a\sigma}|\vec{n}\rangle = \begin{cases} (-1)^{\#_{a\sigma}}|\dots, n_{a\sigma}-1, \dots\rangle & \text{if } n_{a\sigma}=1 \\ 0 & \text{otherwise} \end{cases}; \quad (4)$$

$$c_{a\sigma}^+|\vec{n}\rangle = \begin{cases} (-1)^{\#_{a\sigma}}|\dots, n_{a\sigma}+1, \dots\rangle & \text{if } n_{a\sigma}=0 \\ 0 & \text{otherwise} \end{cases} \quad (5)$$

with $\#_{a\sigma} = \sum_{b\sigma' < a\sigma} n_{b\sigma'}$. Thus, each state is represented as a string of zeros and ones, i.e. the binary decomposition of a given integer number I . Using the identification $|\vec{n}\rangle = |I\rangle$, with $I = 0, \dots, 2^{2N_s} - 1$, each state in the Fock basis can be encoded in a computer using a sequence of $2N_s$ bits or, equivalently, an integer number in a fixed representation. The exponentially growing size of the Fock space will eventually make such representation unpractical. A solution is obtained by decomposing each state according to the existing QNs. For a given set $[\vec{N}_\uparrow, \vec{N}_\downarrow]$ of QNs we then have:

$$\begin{aligned} |\vec{n}\rangle &= \prod_{\alpha=1}^{N_{ud}} \prod_{\sigma=\uparrow\downarrow} |n_1 \dots n_{N_{bit}}\rangle_{\alpha\sigma} \\ &= \begin{cases} |\vec{n}_\uparrow\rangle|\vec{n}_\downarrow\rangle, & \text{if } N_{ud} = 1 \\ |\vec{n}_{1\uparrow}\rangle \dots |\vec{n}_{N_{ud}\uparrow}\rangle |\vec{n}_{1\downarrow}\rangle \dots |\vec{n}_{N_{ud}\downarrow}\rangle, & \text{if } N_{ud} = N_\alpha \end{cases} \end{aligned} \quad (6)$$

so that, if the total number of electrons with spin \uparrow and \downarrow is conserved, any state is identified by two binary sequences of $N_{bit} = N_s$ bits, one per spin orientation. Alternatively, if the number of electrons with spin \uparrow and \downarrow per orbital is conserved, the states are decomposed into two sets of binary sequences (one set per spin orientation), each sequence being made of $N_{bit} = N_s/N_\alpha$ bits. Each binary sequence is associated to a suitable tuple of integer numbers, such as to univocally identify the Fock state: $I \rightarrow [\vec{I}_\uparrow, \vec{I}_\downarrow]$, where $I = 0, \dots, 2^{2N_s} - 1$ and $\vec{I}_\sigma = [I_{1\sigma}, \dots, I_{N_{ud}\sigma}]$ with $I_{\alpha\sigma} = 0, \dots, 2^{N_{bit}} - 1$. Through such decomposition, each state can be described by the smallest bit set compatible with the conserved QNs. This setup generalize the method introduced by Lin and Gubernatis in Ref. 1. The relation between the Fock state index I and its tuple decomposition can be easily inverted:

$$I = I_1 + \sum_{i=2}^{2N_{ud}} I_i 2^{N_{bit}(i-1)}, \quad (7)$$

where we rearranged the tuple as $[\vec{I}_\uparrow, \vec{I}_\downarrow] = [I_1, \dots, I_{2N_{ud}}]$.

Such organization of the Fock states is used to construct a suitable basis for the sectors $\mathcal{S}[\vec{N}_\uparrow, \vec{N}_\downarrow]$. To any given Fock state $|\vec{n}\rangle$ and its integer representation I containing the correct bit decomposition dictated by the QNs it is associated a state $|i\rangle$ and an integer i , with $i = 1, \dots, D_{\mathcal{S}}$, through a suitable *map* $\vec{\mathcal{M}}_{\mathcal{S}}$. In particular, each tuple of integers identifying a Fock state belonging to \mathcal{S} is associated to a new tuple specific for each sector state: $I \in \mathcal{S} = [\vec{I}_\uparrow, \vec{I}_\downarrow] \in \mathcal{S} \xrightarrow{\vec{\mathcal{M}}_{\mathcal{S}}} [\vec{i}_\uparrow, \vec{i}_\downarrow] = i$, where $\vec{i}_\sigma = [i_{1\sigma}, \dots, i_{N_{ud}\sigma}]$ and $i_{\alpha\sigma} = 1, \dots, D_{\alpha\sigma}$. The tuple $[\vec{i}_\uparrow, \vec{i}_\downarrow]$ univocally identifies a basis state $|i\rangle = |\vec{i}_\uparrow, \vec{i}_\downarrow\rangle$ of the sector \mathcal{S} , through a relation similar to (7):

$$i = i_{1\uparrow} + \sum_{\sigma} \sum_{l=2}^{N_{ud}} (i_{l\sigma} - 1) \prod_{\alpha=1}^{l-1} D_{\alpha\sigma} \quad (8)$$

2.4. The Hamiltonian matrix

The matrix representing the system Hamiltonian in the Fock space has a block diagonal structure in presence of a given set of conserved QNs. Each block corresponds to the Hamiltonian of a sector $\mathcal{S}[\vec{N}_\uparrow, \vec{N}_\downarrow]$. The analysis of the spectrum, thus, reduces to the recursive analysis of the sector Hamiltonians. In each sector, the Hamiltonian of the system has the following general form:

$$H_{\mathcal{S}}^e = H_d + H_\uparrow \otimes \mathbb{1}_\downarrow + \mathbb{1}_\uparrow \otimes H_\downarrow + H_{nd}. \quad (9)$$

H_d is a diagonal term containing the local part of the Hamiltonian, including the density-density terms of the interaction. The H_σ components describe all the hopping processes of the electrons with spin $\sigma = \uparrow, \downarrow$. Finally the term H_{nd} contains all the remaining non-diagonal elements which do not fit in the previous two components, e.g. the spin-exchange and pair-hopping interaction terms. If the QNs are conserved per orbital, i.e. if $H_{nd} \equiv 0$ and no inter-orbital local hopping terms are present, each H_σ further splits into a sum of smaller terms:

$$H_\sigma = \sum_{\alpha=1}^{N_\alpha} \mathbb{1}_{1\sigma} \otimes \dots \otimes H_{\alpha\sigma} \otimes \dots \otimes \mathbb{1}_{N_\alpha\sigma}$$

Each term of the Hamiltonian matrix is constructed independently iterating on one or more components of the sector basis states. For example, the construction of the matrices $H_{\alpha\sigma}$ only involves iterations over the components $|i_{\alpha\sigma}\rangle$ of the sector basis. In general we have:

$$\begin{aligned} \langle \vec{i}_\uparrow \vec{i}_\downarrow | H_{\mathcal{S}}^e | \vec{j}_\uparrow \vec{j}_\downarrow \rangle &= \langle \vec{i}_\uparrow \vec{i}_\downarrow | H_d + H_\uparrow \otimes \mathbb{1}_\downarrow + \mathbb{1}_\uparrow \otimes H_\downarrow + H_{nd} | \vec{j}_\uparrow \vec{j}_\downarrow \rangle \\ &= \langle \vec{i}_\uparrow \vec{i}_\downarrow | H_d | \vec{i}_\uparrow \vec{i}_\downarrow \rangle + \\ &\quad \langle \vec{i}_\uparrow | H_\uparrow | \vec{j}_\uparrow \rangle \delta_{\vec{i}_\downarrow \vec{j}_\downarrow} + \langle \vec{i}_\downarrow | H_\downarrow | \vec{j}_\downarrow \rangle \delta_{\vec{i}_\uparrow \vec{j}_\uparrow} + \\ &\quad \langle \vec{i}_\uparrow \vec{i}_\downarrow | H_{nd} | \vec{j}_\uparrow \vec{j}_\downarrow \rangle \end{aligned} \quad (10)$$

For very large systems, storing the Hamiltonian matrix in the memory can be highly inefficient. In such cases, Krylov or Lanczos methods^{1,38,43,44} can be implemented using a

storage-free algorithm, performing the necessary linear operations on-the-fly. This solution has generally a negative impact onto the execution time, however this can be well compensated by scaling in a massively parallel framework.

3. Matrix-vector product: parallel algorithms

The bottleneck of any Lanczos based diagonalization is the execution of matrix-vector product (MVP) operations, which often takes up to the 90% of the execution time. For any given sector \mathcal{S} the MVP of the Hamiltonian matrix times an arbitrary vector is $|w\rangle = H_{\mathcal{S}}^e|v\rangle$ or, projecting onto the sector basis, $w_i = \sum_j [H_{\mathcal{S}}^e]_{ij} v_j$. Distributing the burden of the MVP across multiple processors can dramatically improve ED calculations and unlock access to larger systems. Yet, the MVP heavily relies on communication among different processors, making the design of efficient parallel algorithms a non-trivial task. In the following, we discuss algorithms based on the distributed memory *Message Passing Interface* (MPI) framework.

3.1. The *MPI_AllGatherV* algorithm

A simple and generic parallel algorithm is constructed as follows. Let us consider the expansion of the vector $|v\rangle$ onto the sector basis $|v\rangle = \sum_i v_i |i\rangle$. The vector elements v_i are distributed across the \mathbf{p} processes in data chunks of $\mathbf{Q} = D_{\mathcal{S}}/\mathbf{p} + \mathbf{R}$ length, with $\mathbf{R}=\text{mod}(D_{\mathcal{S}}, \mathbf{p})$ for the first CPU and $\mathbf{R}=0$ otherwise. In order to distribute the MVP operation among the processes, we assign a share of \mathbf{Q} rows of the matrix $H_{\mathcal{S}}^e$ to each process, consistently with the splitting of the vector $|v\rangle$. In doing that, it is important to distinguish between *local* and *non-local* elements of the vector, i.e. the share of the vector which resides in the memory of a given process and the remaining parts which live on the memory of the other processes.

As such, the result of the MVP consists in two contributions. The first comes from the product of the $\mathbf{Q} \times \mathbf{Q}$ diagonal blocks of $H_{\mathcal{S}}^e$ and the local parts of the vector $|v\rangle$. This term of the product is executed locally on each process, i.e. without any inter-process communication. The second contribution comes from the multiplication of the remaining elements of the matrix share and the vector. Due to its non-local nature, this term of the MVP requires to reconstruct the distributed vector $|v\rangle$. This task is achieved through a call to the MPI function `MPI_AllGatherV`, which execute a communication of the vector shares from each process to all the other processes.

Although conceptually simple, the scaling analysis of this algorithm reveals a quick saturation already for a number \mathbf{p} of processors of the order of ten. Indeed, the gain deriving from the decreased size \mathbf{Q} of the vector share ($\simeq 1/\mathbf{p}$) is rapidly balanced and overcome by the inter-processors communication in `MPI_AllGatherV` which amount to a massive data transfer among processors. Such communication congestion ultimately prevents to achieve a good parallel scaling.

3.2. The *MPI_AllToAllV* algorithm

An improved, yet less generic, parallel algorithm can be devised exploiting the basis states decomposition introduced above. In the sector basis $|\vec{i}_{\uparrow}\vec{i}_{\downarrow}\rangle$ a generic vector $|v\rangle$ can be

decomposed as:

$$|v\rangle = \sum_i v_i |i\rangle = \sum_{\vec{i}_\uparrow, \vec{i}_\downarrow} v_{\vec{i}_\uparrow, \vec{i}_\downarrow} |\vec{i}_\uparrow, \vec{i}_\downarrow\rangle = \sum_{i_\uparrow=1}^{D_\uparrow} \sum_{i_\downarrow=1}^{D_\downarrow} v_{i_\uparrow, i_\downarrow} |i_\uparrow\rangle |i_\downarrow\rangle \quad (11)$$

where in the last equality we used the relation (8) to rearrange the tuples of indices $\vec{i}_\uparrow, \vec{i}_\downarrow$ and the states $|\vec{i}_\uparrow, \vec{i}_\downarrow\rangle$ in, respectively, a pair of scalar indices i_\uparrow, i_\downarrow and states of the form $|i_\uparrow\rangle |i_\downarrow\rangle$. The sector basis states are ordered so that the spin- \uparrow index runs faster than the spin- \downarrow one. Thus, any vector $|v\rangle$ can be represented as a matrix whose columns correspond to a set of spin- \uparrow components for a given fixed spin- \downarrow configuration:

$$\{v_i\}_{i=1, \dots, D_\uparrow D_\downarrow} \doteq \begin{pmatrix} v_{1_\uparrow 1_\downarrow} \\ \vdots \\ v_{D_\uparrow 1_\downarrow} \\ \vdots \\ v_{1_\uparrow D_\downarrow} \\ \vdots \\ v_{D_\uparrow D_\downarrow} \end{pmatrix} = \begin{pmatrix} v_{1_\uparrow 1_\downarrow} & \dots & v_{1_\uparrow D_\downarrow} \\ v_{2_\uparrow 1_\downarrow} & \dots & v_{2_\uparrow D_\downarrow} \\ \dots & \dots & \dots \\ v_{D_\uparrow 1_\downarrow} & \dots & v_{D_\uparrow D_\downarrow} \end{pmatrix} \quad (12)$$

Each vector is distributed across the MPI processes such as a number $Q_\downarrow = D_\downarrow/p$ of columns is assigned to each core. If present, the rest $R_\downarrow = \text{mod}(D_\downarrow, p)$ is reassigned to the first R_\downarrow processes. This partitioning corresponds to distribute $Q = D_\uparrow \times Q_\downarrow$ vector elements to each process. Each term in (10) contributing to the MVP is evaluated separately.

3.2.1. The H_d term

The diagonal term H_d of the Hamiltonian is distributed among processes assigning Q rows, i.e. elements, to each core. Notably, the multiplication $H_d|v\rangle$ takes place locally in the memory on each process, i.e. with no need of further MPI communication.

3.2.2. The $H_\uparrow \otimes \mathbb{1}_\downarrow$ term

The contribution of the term $H_\uparrow \otimes \mathbb{1}_\downarrow$ to the MVP involves only \uparrow -electrons elements, for any fixed configuration of the spin- \downarrow . In the MVP, this corresponds to run along the elements of each column of the matrix (12). The proposed MPI decomposition ensures that these elements are stored contiguously in the memory of each process. As such, like the diagonal term H_d , this term of the MVP can be performed locally in the memory of any processor, provided the (small) Hamiltonian H_\uparrow is known to each process or it can be evaluated on-the-fly.

3.2.3. The $\mathbb{1}_\uparrow \otimes H_\downarrow$ term

The product with the term $\mathbb{1}_\uparrow \otimes H_\downarrow$ involves \downarrow -electrons elements, for any fixed spin- \uparrow configuration. In the MVP this corresponds to run along the rows of the matrix (12),

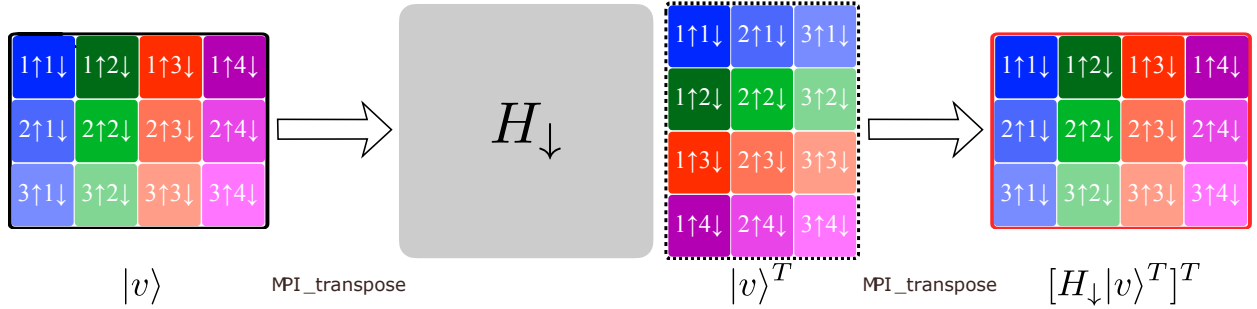


Figure 1: (Color online) Schematic representation of the MVP for the $l_\uparrow \otimes H_\downarrow$ term of the sector Hamiltonian. In this example the sector dimensions are $D_S = D_\uparrow \times D_\downarrow = 3 \times 4$. We assume to have $p=4$ processors. The components of the vector are indicated by their index $v_{i_\uparrow i_\downarrow} \rightarrow i_\uparrow i_\downarrow$. Each column of the initial vector $|v\rangle$ correspond to a different \downarrow configuration, indicated by different colors. The shades of the same color corresponds to different \uparrow configuration. The columns are distributed to the processors. The distributed vector is parallel transposed so that each column correspond a different up configuration and belong to one processor. The MVP $|w\rangle^T = H_\downarrow|v\rangle^T$ can then be performed locally in the memory. The result $|w\rangle$ is obtained transposing back the resulting into the original format.

ultimately leading to a highly non-local access to the memory. In a serial implementation this introduces only a minor performance degradation due to irregular cache access. However, in a parallel algorithm such non-locality represents a serious bottleneck, which requires massive MPI communication to transfer columns among different processes. A solution to such problem is to exchange the \uparrow - and \downarrow -configuration indices $[\vec{i}_\uparrow, \vec{i}_\downarrow] \rightarrow [\vec{i}_\downarrow, \vec{i}_\uparrow]$, corresponding to an actual transposition of the matrix (12). The execution of transposed MVP recover locality in the processors memory.

The key issue is thus reduced to perform a collective transposition of a data set, which in turn requires a suitable all-to-all communication. To this purpose, the MPI library makes available a parallel procedure, `MPI_AlltoAllv`²⁷, which transfers data such that the j -block, sent from the process i , is received by process j and placed as block i . The corresponding communication pattern is schematically depicted in Fig. 6. This *parallel transposition* involves the minimum amount of data transfer necessary to execute the MVP, removing the communicational congestion and unlocking optimal parallel scaling. Details of the implementation are given in Sec. 6.7.

Summarizing, the MVP of the \downarrow -electrons part of the Hamiltonian proceeds in three steps: i) the vector $|v\rangle$ is transposed using collective MPI communication; ii) the multiplication is performed locally on each process; iii) the resulting vector is transposed back and added up to the result, see Fig. 1.

3.2.4. The H_{nd} term

The last contribution to the MVP is from the non-diagonal term H_{nd} . This matrix contains elements which can not be reduced to any favourable form to perform a parallel MVP. As such, the execution of the MVP for this term necessarily relies on the `MPI_AllgatherV`-

algorithm, discussed above. To this end, the matrix H_{nd} gets row-distributed among all processes assigning \mathbf{Q} rows to each core. The inclusion of this term is expected to spoil to some extent the scalability of the parallel MVP algorithm.

3.3. Dynamical correlation functions

The knowledge of the Hamiltonian spectrum, or just of its lowest part, provides the means to evaluate generic dynamical correlation functions of the form: $G_{\mathcal{O}} = \langle \mathcal{T}_{\pm}[\mathcal{O}(t)\mathcal{O}^+] \rangle$, where $\mathcal{O}(t) = e^{iHt}\mathcal{O}e^{-iHt}$ is an operator in the Heisenberg representation, \mathcal{T}_{\pm} is the time-ordering operator for fermions (+) or bosons (-) and $\langle \mathcal{O} \rangle = \frac{1}{Z} \text{Tr} [e^{-\beta H} \mathcal{O}]$, $Z = \sum_n e^{-\beta E_n}$, is the thermodynamic average. Performing a Fourier transformation and using spectral theorem, the expression for $G_{\mathcal{O}}$ can be recasted in the more convenient form:

$$\begin{aligned} G_{\mathcal{O}}(z) &= \langle \mathcal{O} \frac{1}{z - (H - E_0)} \mathcal{O}^+ \rangle \mp \langle \mathcal{O}^+ \frac{1}{z + (H - E_0)} \mathcal{O} \rangle \\ &= \frac{1}{Z} \sum_n e^{-\beta E_n} \langle \psi_n | \mathcal{O} \frac{1}{z - (H - E_0)} \mathcal{O}^+ | \psi_n \rangle \mp \langle \psi_n | \mathcal{O}^+ \frac{1}{z + (H - E_0)} \mathcal{O} | \psi_n \rangle \\ &= \frac{1}{Z} \sum_n e^{-\beta E_n} \sum_m \frac{\langle \psi_n | \mathcal{O} | \psi_m \rangle \langle \psi_m | \mathcal{O}^+ | \psi_n \rangle}{z - (H - E_0)} \mp \frac{\langle \psi_n | \mathcal{O}^+ | \psi_m \rangle \langle \psi_m | \mathcal{O} | \psi_n \rangle}{z + (H - E_0)} \end{aligned} \quad (13)$$

where $z \in \mathbb{C}$, $|\psi_n\rangle$ are the eigenstates of the Hamiltonian H and E_0 is the groundstate energy. A key simplification in the evaluation of any dynamical correlation function is obtained using the Lanczos procedure. Introducing a suitable Krylov basis the Hamiltonian matrix takes a tri-diagonal form, which allows to evaluate an arbitrary number of terms in the sum over the internal excited states $|\psi_m\rangle$. For example, let's consider the normalized initial state $|\phi_n\rangle = \mathcal{O}^+ |\psi_n\rangle / \sqrt{\langle \psi_n | \mathcal{O} \mathcal{O}^+ | \psi_n \rangle}$ with $|\psi_n\rangle \in \mathcal{S}$ and the Krylov basis $\mathcal{K}_N(|\phi_n\rangle) = \{|\phi_n\rangle, H|\phi_n\rangle, \dots, H^N|\phi_n\rangle\} \equiv \{|v_0^n\rangle, |v_1^n\rangle, \dots, |v_N^n\rangle\}$ with $1 \ll N \ll \mathcal{D}_{\mathcal{S}}$.

Any eigenstate $|\psi_n\rangle$ is decomposed along the $\mathcal{K}_N(|\phi_n\rangle)$ basis as: $|\psi_n\rangle = \sum_i \langle v_i^n | \psi_n \rangle |v_i^n\rangle = \sum_i a_i^n |v_i^n\rangle$. Using this decomposition, we can evaluate the operator components $\langle \psi_m | \mathcal{O}^+ | \psi_n \rangle = \sqrt{\langle \psi_n | \mathcal{O} \mathcal{O}^+ | \psi_n \rangle} a_m^{n*}$ and thus:

$$\langle \psi_n | \mathcal{O} \frac{1}{z - (H - E_0)} \mathcal{O}^+ | \psi_n \rangle \simeq \langle \psi_n | \mathcal{O} \mathcal{O}^+ | \psi_n \rangle \sum_{m=1}^N \frac{|a_m^n|^2}{z - (E_m - E_0)} \quad (14)$$

Repeating the same decomposition for each term in Eq. 13, we obtain the following approximation to $G_{\mathcal{O}}$:

$$\begin{aligned} G_{\mathcal{O}}(z) &= \frac{1}{Z} \sum_n e^{-\beta E_n} G_{\mathcal{O}}^n(z) \\ G_{\mathcal{O}}^n(z) &\simeq \sum_{m=1}^N \frac{\langle \psi_n | \mathcal{O} \mathcal{O}^+ | \psi_n \rangle |a_m^n|^2}{z - (E_m - E_0)} \mp \frac{\langle \psi_n | \mathcal{O}^+ \mathcal{O} | \psi_n \rangle |a_m^n|^2}{z + (E_m - E_0)} \end{aligned} \quad (15)$$

In many concrete situations one has to deal with non-diagonal dynamical correlation functions, e.g.: $G_{AB}(z) = \langle A^+ \frac{1}{z - (H - E_0)} B \rangle$, which can not be treated by the procedure

outlined above. A simple solution is to consider auxiliary operators of the form $\mathcal{O} = \mathcal{A} + \mathcal{B}$ and $\mathcal{P} = \mathcal{A} - i\mathcal{B}$. Using simple algebra it is then straightforward to obtain the desired function $G_{\mathcal{AB}}$ from the evaluation of $G_{\mathcal{O}}$ and $G_{\mathcal{P}}$:

$$G_{\mathcal{AB}} = \frac{1}{2} [G_{\mathcal{O}} + G_{\mathcal{P}} - (1 - i)G_{\mathcal{A}} - (1 + i)G_{\mathcal{B}}]$$

4. Electron-phonon coupling

The quantum impurity model (1) can be extended to include electron-phonon coupling. The impurity Hamiltonian takes the form: $\hat{H} = \hat{H}_e + \hat{H}_{e-ph} + \hat{H}_{ph}$, where $H_{ph} = \omega_0 b^\dagger b$, $H_{e-ph} = \sum_{\alpha\sigma} g_\alpha c_{\alpha\sigma}^\dagger c_{\alpha\sigma} (b + b^\dagger)$. The presence of additional, bosonic, degrees of freedom introduces major changes to the ED algorithm. However, such modifications do not spoil the essential aspects of the parallel algorithms outlined above.

4.1. Fock space

The Fock space should be extended to include the presence of the phonons. In order to deal with the unbounded dimensions of the local Hilbert space of the phonons we introduce a cut-off N_{ph} to the number of available phonons. The Fock space of a system of M_{ph} phonons is $\mathcal{F}_{ph} = \bigoplus_{n=0}^{M_{ph}} S_+ \mathcal{H}_{ph}^{\otimes n}$, with $\mathcal{H}_{ph} = \{|0\rangle, |1\rangle, \dots, |N_{ph}\rangle\}$ is the local phonon Hilbert space and S_+ the symmetrization operator. The Fock space is given by the tensor product of the electronic and phononic spaces: $\mathcal{F} = \mathcal{F}_e \otimes \mathcal{F}_{ph}$. In the following we reduce to the case of a single phonon mode $M_{ph} = 1$, localized in real space at the impurity site. As such the dimension of the phonon Fock space is given by $D_{ph} = N_{ph} + 1$.

The coupling to phonons does not break the electronic QNs conservation nor it adds novel symmetries. Thus, the Fock space factorizes into novel sectors given by the product of any electronic sector and the phonons Hilbert space. Each sector is then identified by the tuple $[\vec{N}_\uparrow, \vec{N}_\downarrow]$ and has dimensions $\dim(\mathcal{S}[\vec{N}_\uparrow, \vec{N}_\downarrow]) = D_\uparrow D_\downarrow D_{ph} \equiv D_S$.

4.2. Basis states

According to this construction, the Fock basis of the electron-phonon system is composed of product states of the form $|\vec{n}, p\rangle = |n_{1\uparrow}, \dots, n_{N_s\uparrow}, n_{1\downarrow}, \dots, n_{N_s\downarrow}\rangle |p\rangle$, with $p = 0, 1, \dots, N_{ph}$. The electronic and phononic creation (annihilation) operators, respectively, $c_{\alpha\sigma}^\dagger$, a^\dagger ($c_{\alpha\sigma}$, a) act separately on the electronic and phononic part of the states. This separation of the Fock basis ensures that all the observations concerning the electronic configurations hold unaltered. In particular, each state $|\vec{n}\rangle$ is repeated D_{ph} times. Consequently, we identify each Fock state by means of an integer index and an extended tuple $I \rightarrow [I_e, I_{ph}] = [\vec{I}_\uparrow, \vec{I}_\downarrow, I_{ph}]$, where $I_{ph} = 0, \dots, N_{ph}$ and I_e identify the electronic Fock state. The relation between the Fock state index I and the tuple reads:

$$I = I_1 + \sum_{i=2}^{2N_{ud}} I_i 2^{(i-1)N_{bit}} + I_{ph} 2^{2N_s} \quad (16)$$

In complete analogy, we use of the map $\vec{\mathcal{M}}_{\mathcal{S}}$ to build a basis for sector $\mathcal{S}[\vec{N}_{\uparrow}, \vec{N}_{\downarrow}]$, such that $I \in \mathcal{S} = [\vec{I}_{\uparrow}, \vec{I}_{\downarrow}, I_{ph}] \in \mathcal{S} \xrightarrow{\vec{\mathcal{M}}_{\mathcal{S}}} [\vec{i}_{\uparrow}, \vec{i}_{\downarrow}, i_{ph}] = i$, where $i_{\alpha\sigma} = 1, \dots, D_{ph}$. The tuple $[\vec{i}_{\uparrow}, \vec{i}_{\downarrow}, i_{ph}]$ identifies a state $|i\rangle = |\vec{i}_{\uparrow}, \vec{i}_{\downarrow}\rangle|i_{ph}\rangle$ of the sector \mathcal{S} through the relation:

$$i = i_{1\uparrow} + \sum_{\sigma} \sum_{\alpha=2}^{N_{ud}} (i_{\alpha\sigma} - 1) \prod_{\beta=1}^{\alpha-1} D_{\beta\sigma} + (i_{ph} - 1)D_{\uparrow}D_{\downarrow}. \quad (17)$$

4.3. Hamiltonian construction

In each sector \mathcal{S} the Hamiltonian matrix of the electron-phonon coupled system has the following expression:

$$H_{\mathcal{S}} = \mathbb{P}^{ph} \otimes H_{\mathcal{S}}^e + H^{ph} \otimes \mathbb{I}^{el} + H_{e-ph}^{ph} \otimes H_{e-ph}^e \quad (18)$$

where $H_{\mathcal{S}}^e$ is the electronic sector Hamiltonian, H^{ph} is the phonon Hamiltonian. H_{e-ph}^{ph} and H_{e-ph}^e are, respectively, the phononic and electronic parts of the electron-phonon coupling term. Because of the factorization of the basis states, the construction of the electronic part of the Hamiltonian proceed as outlined above. The H^{ph} term is diagonal in the phonon basis and independent of the electronic configuration. The electron-phonon coupling term $H_{e-ph}^{ph} \otimes H_{e-ph}^e$ can be factorized. The electronic part is diagonal, as the component H_{e-ph}^e is proportional to the electronic density operators. However, the phonon factor H_{e-ph}^{ph} , being linear in the phonon displacement operator $\hat{x} = (a^{\dagger} + a)$, is off-diagonal in the phonon states.

$$\begin{aligned} \langle \vec{i}_{\uparrow}\vec{i}_{\downarrow} | \langle i_{ph} | H_{\mathcal{S}} | \vec{j}_{\uparrow}\vec{j}_{\downarrow} \rangle | j_{ph} \rangle &= \langle \vec{i}_{\uparrow}\vec{i}_{\downarrow} | H_{\mathcal{S}}^e | \vec{j}_{\uparrow}\vec{j}_{\downarrow} \rangle \delta_{i_{ph}j_{ph}} + \\ &\delta_{\vec{i}_{\uparrow}\vec{j}_{\uparrow}} \delta_{\vec{i}_{\downarrow}\vec{j}_{\downarrow}} \langle i_{ph} | H^{ph} | i_{ph} \rangle + \\ &\langle \vec{i}_{\uparrow}\vec{i}_{\downarrow} | H_{e-ph}^e | \vec{i}_{\uparrow}\vec{i}_{\downarrow} \rangle \langle i_{ph} | H_{e-ph}^{ph} | j_{ph} \rangle \end{aligned} \quad (19)$$

4.4. Parallel matrix-vector product

The factorization of the electrons and phonons configurations in the basis states allows to introduce only few changes to the MVP algorithm, designed to optimize the parallel execution. The most important step concerns the distribution of the vectors among the processes. To this end, we observe that the vector decomposition along the sector basis is such that the electronic configurations are ‘‘repeated’’ D_{ph} number of times:

$$|v\rangle = \sum_{i, i_{ph}} v_{i, i_{ph}} |i\rangle |i_{ph}\rangle = \sum_{i_{\uparrow}=1}^{D_{\uparrow}} \sum_{i_{\downarrow}=1}^{D_{\downarrow}} \sum_{i_{ph}=1}^{D_{ph}} v_{i_{\uparrow}, i_{\downarrow}, i_{ph}} |i_{\uparrow}\rangle |i_{\downarrow}\rangle |i_{ph}\rangle \quad (20)$$

Thus, each vector is distributed among the MPI processes such as $\mathbb{Q}_{\downarrow}^{ph} \times D_{ph} = D_{\downarrow}/\mathfrak{p} \times D_{ph}$ columns, i.e. D_{ph} copies of the \mathbb{Q}_{\downarrow} electronic configurations, are assigned to each core. Each process holds $\mathbb{Q}^{ph} = D_{\uparrow} \times \mathbb{Q}_{\downarrow} \times D_{ph} \equiv D_{\uparrow} \times \mathbb{Q}_{\downarrow}^{ph}$ elements.

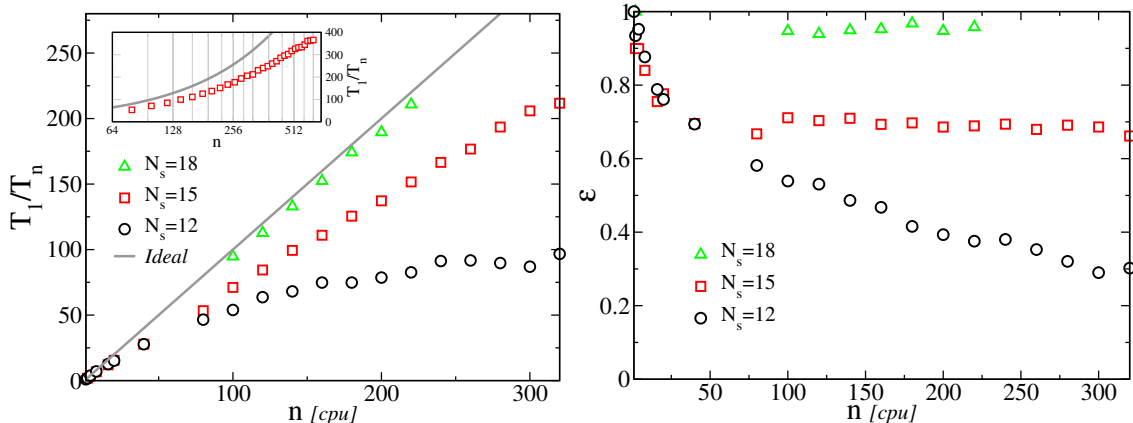


Figure 2: (Color online) Left: Parallel speed-up T_1/T_n as a function of the CPUs number n . Data are for systems with increasing number of levels $N_s = 12, 15$ and 18 . The ideal scaling (solid gray line) is reported for comparison. The parallel gain saturates at $n \simeq 256$ for $N_s = 12$, it shows sub-ideal behavior for $N_s = 15$ and nearly ideal scaling for $N_s = 18$. Data for $N_s = 18$ are normalized to $n = 2$. Inset: Parallel speed-up as a function of CPUs number for $N_s = 15$ in a wider range of n and on a semi-log scale. The results shows the saturation of the parallel gain for $n > 512$. Right: Parallel efficiency $\epsilon = T_1/nT_n$ as a function of the CPUs number n . Data as in left panel.

Then, for any fixed phonon configuration, the execution of the MVP for the purely electronic part of the Hamiltonian proceeds along the same lines. The product with the phonon Hamiltonian H^{ph} , diagonal in the electronic states, only involves iterations along the phonon index for all the electronic elements residing on each processor, i.e. it is local in the memory. Finally, according to the vector distribution among the processors, the product with the electron-phonon Hamiltonian is straightforward. The H_{e-ph}^e Hamiltonian is diagonal and distributed to the processors in shares of size Q rows, so its contribution is local in the memory. Finally, the term H_{e-ph}^{ph} , known to each process, connects columns of electronic elements Q with different phonon index, yet residing in the memory of the same process and requiring no further change to the MVP algorithm.

5. Benchmarks

We present some benchmark results for the massively parallel ED algorithm outlined above. The calculations have been performed on HPC cluster, using Intel Xeon E5-2680 v2 processors with 2 sockets, 10 cores, 2 threads per core and 40 GB RAM. We considered a multi-orbital quantum impurity model with a total of N_s electronic levels. The impurity host N_α orbitals, each coupled via an hopping amplitude to N_b bath levels, with random energies in the interval $[-2D, 2D]$, with $D = 1$ setting the energy unit. The tests have been executed using total spin \uparrow, \downarrow electrons occupation QNs in the half-filling sector $N_\uparrow = N_\downarrow$. This setup corresponds to the largest possible sector dimension, which is ideal to test scaling properties of the algorithm. Timing is relative to the evaluation of the lowest state of the spectrum, using Lanczos or P-Arpack⁴⁴ algorithm with on-the-fly evaluation of the MVP, i.e. without

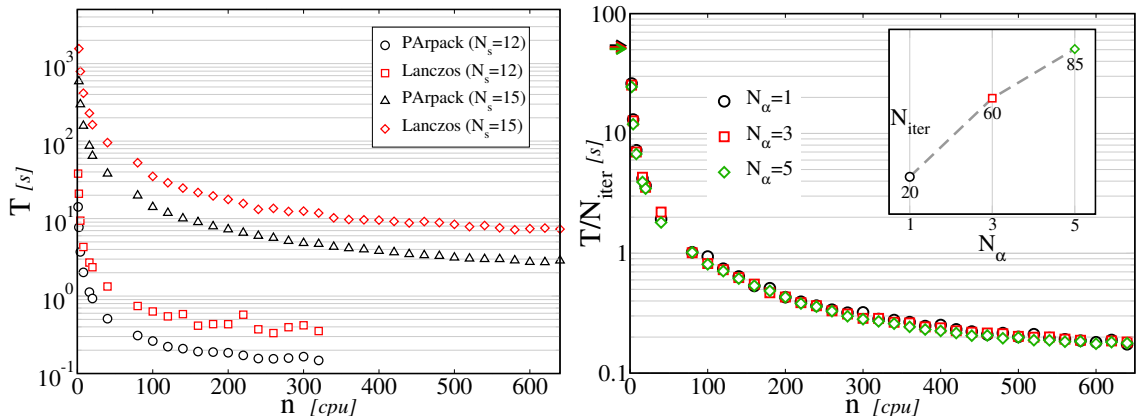


Figure 3: (Color online) Left panel: Total execution time T as a function of the number of CPUs n , for systems of $N_s = 12, 15$ levels. Data compare results obtained with P-Arpack (black circles and triangles) against simple Lanczos (red squares and diamonds) methods. Right panel: Average execution time for a single Lanczos iteration T/N_{iter} as a function of CPUs number n . Data are for a system of $N_s = 15$ levels with a number of orbitals $N_\alpha = 1, 3, 5$. The data show that single Lanczos iteration time is essentially independent of the orbitals number N_α . Inset: number of Lanczos iterations N_{iter} for a single groundstate calculation as a function of orbitals number N_α . Data show that the iterations number linearly increases with the N_α and so does the total execution time T .

storage of the Hamiltonian. In order to reduce the intrinsic errors, we performed repeated calculations for different realizations of the bath energy distribution. The data presented in this section are averaged over 10 realizations.

The speed-up of the parallel algorithm and its efficiency are reported in Fig. 2 for an increasing number of total electronic levels N_s . For a system with $N_s = 12$, the parallel gain rapidly saturates for $n \simeq 250$ cpus. Indeed, for such small system the ratio between calculation and communication time quickly becomes unfavourable, leading to a premature saturation of the performances. This is further underlined by the decreasing behavior of the parallel efficiency ε reported in the right panel. The scaling improves for larger systems. In particular, we observed a sub-linear scaling for systems of $N_s = 15$, which displays a saturation tendency only for the largest accessible number of processes (see inset). For this size, the parallel efficiency shows a nearly constant behavior up to the largest number of processor. Finally, for the largest system with $N_s = 18$ we observed a quasi ideal scaling and efficiency near one in the entire range of cpu number analyzed.

In order to test the solidity of the scaling with respect to the intrinsic properties of the Lanczos algorithm, we compared the single vector Lanczos implementation with respect to a fully fledged P-Arpack algorithm⁴⁴. For the P-Arpack calculations we used a block of $n_{cv} = 10$ vectors, which we observed to optimize the execution of our program. The memory footprint as well as the number of matrix-vector operations among the two methods are very different, potentially leading to dissimilar scaling behavior. The results in the left panel of Fig. 3 reveal that the scaling of the two methods is indeed similar, i.e. the same order of magnitude. Interestingly however, despite its higher complexity, the more optimized

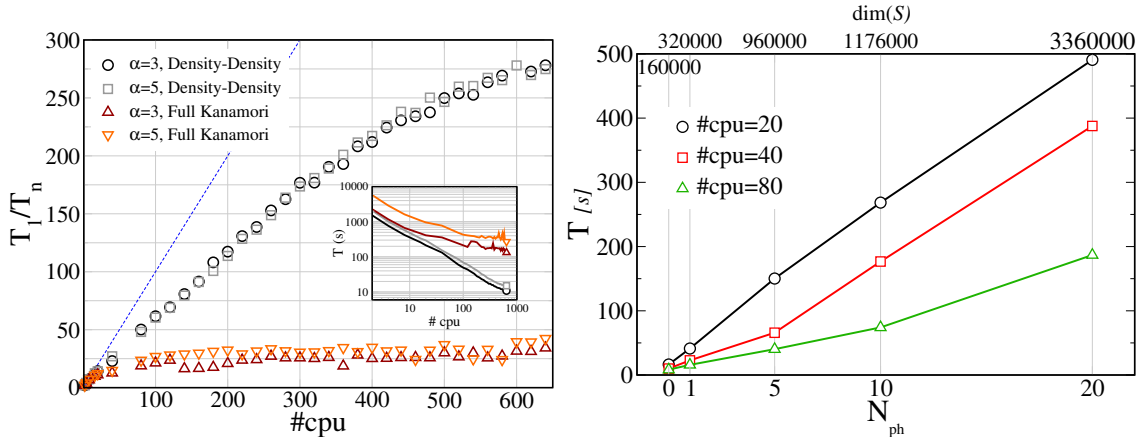


Figure 4: (Color online) Left panel: Parallel speedup of the ED algorithm as a function of the number of processes for a single ground-state calculation. Data are obtained using P-Arpack ($ncv = 10$), for a number of orbitals $N_\alpha = 3, 5$, $N_s = 15$ and two type of interaction terms: Ising or density-density (black circles and gray squares) and full Kanamori including spin-flipping and pair-exchange (red up triangles and orange down triangles). Ideal scaling (dotted blue line) is reported for comparison. The data show that inclusion of non-diagonal Hamiltonian terms H_{nd} quickly saturates the scaling. Right panel: Total execution time for the groundstate calculation as a function of the number of phonons N_{ph} . The plot displays the linear scaling of the algorithm with N_{ph} . Data are obtained using P-Arpack ($ncv = 10$), for $N_s = 12$ in the half-filled sector $N_\uparrow = N_\downarrow = 6$ for total occupation per spin QNs. The top x-axis show to the dimensions of the sector $\dim(S)$ for a given number of phonons. $N_{ph} = 0$ corresponds to the purely electronic problem.

P-Arpack algorithm performed consistently better than the plain Lanczos method.

A crucial aspect towards application of the algorithm is the scaling behaviour with respect to the number of orbitals. The multi-orbital interaction includes terms which are not diagonal in the electronic configurations, such as spin-flip and pair-hopping. These terms have a possible detrimental impact on the parallel scaling, thus we temporarily exclude their contributions and we will analyze their influence separately. In multi-orbital systems the hopping matrices include more terms with respect to the single orbital, due to the presence of several hopping channels among orbitals. In order to characterize quantitatively these aspects we studied the scaling of the algorithm as a function of an increasing number of orbital N_α , see the right panel of Fig. 3. Our results show that the single Lanczos iteration time is essentially independent of the number of orbitals. However, the number of iterations required to determine the lowest eigenstate increases linearly with the number of orbitals, see inset. We conclude that, although the resulting total time has an excellent sub-linear scaling with the number of processes, it linearly depends on the number of orbitals, i.e. the more the orbitals the larger the solution time for a fixed number of processes.

As mentioned above, we analyzed the effect of non-diagonal interaction terms on the scaling behavior of our algorithm. The pair-hopping and spin-exchange terms cannot be reduced to hopping events involving a single spin orientation. As such we can not take advantage of the special properties of the basis states to perform the parallel MVP, possibly spoiling the nearly optimal scaling observed for the case of density-density interaction only. In order to

quantify this effect in Fig. 4 we compare the speed-up behavior of the density-density and full Kanamori interaction, in two systems of 3 and 5 orbitals. As before, the density-density interaction has a sub-linear scaling, which saturates around $n > 600$ processes. The behavior of the full Kanamori case is however very different. An initial good speed-up obtained with few tens of processes, quickly saturates to a value of 50 – 75 for any number of CPU $n > 100$. In fact, above this threshold the burden of the MPI communication needed to reconstruct the whole vector and perform the product for H_{nd} becomes predominant and prevents further improvement of the scaling.

The scaling properties of the parallel algorithm are mostly influenced by the dimensions of the sector associated to a specified set of QNs as well as the sparseness of the hopping Hamiltonian matrices, which is partially controlled by the number of orbitals. Thus, the scaling for the case of orbital resolved QNs is qualitatively similar to the results discussed above, provided the sector dimensions are equal, a condition that is fulfilled only for larger value of N_s .

Finally, we discuss the influence on the scaling of the electron-phonon coupling. The presence of the phonons leads to a linear in D_{ph} increase of the sector dimension. In addition, it largely influences the parallel MVP algorithm by introducing slightly detrimental effects. The product with the electronic part of the Hamiltonian, i.e. the most time consuming part of the MVP algorithm, is repeated for each phonon configuration thus we expect an almost linear scaling of the performances with the number of phonons. This expectation is confirmed by the results reported in Fig. 4, where we present the scaling of the ED algorithm with the number of phonons N_{ph} for a system with $N_s = 12$ in the half-filling sector $N_{\uparrow} = N_{\downarrow}$ and total occupation per spin QNs.

6. Library description and implementation

The structure of the library is schematically represented in Fig. 5, using a simplified Unified Modeling Language (UML) diagram. The entire library is written in Fortran using object oriented programming within a modules structure. The Fortran interface is provided by the top-end module exposing to the end-user the procedures required to setup and solve a quantum impurity problem. The Python API are provided by a pure Python module `edipy`. The Python binding is built using an interface module created by `numpy.f2py` from a suitable Fortran layer. In what follows we describe in more details the structure and the implementation of the most relevant parts of the EDIpack library.

6.1. Sparse matrix class

A sparse matrix storage is performed using a dedicated custom class, contained in the `SPARSE_MATRIX` module. The class defines a `sparse_matrix_csr` object as a simplified hash-table. The keys corresponds to the rows of the matrix while the value is associated to a pair dynamical arrays, containing values and columns location of the non-zero elements of the sparse matrix. The `sparse_matrix_csr` object can be stored either serially, i.e. one copy per process, or be parallel distributed assigning a number of keys/values to each process. The elements are progressively stored in the dynamic arrays using `sp_insert_element` procedure,

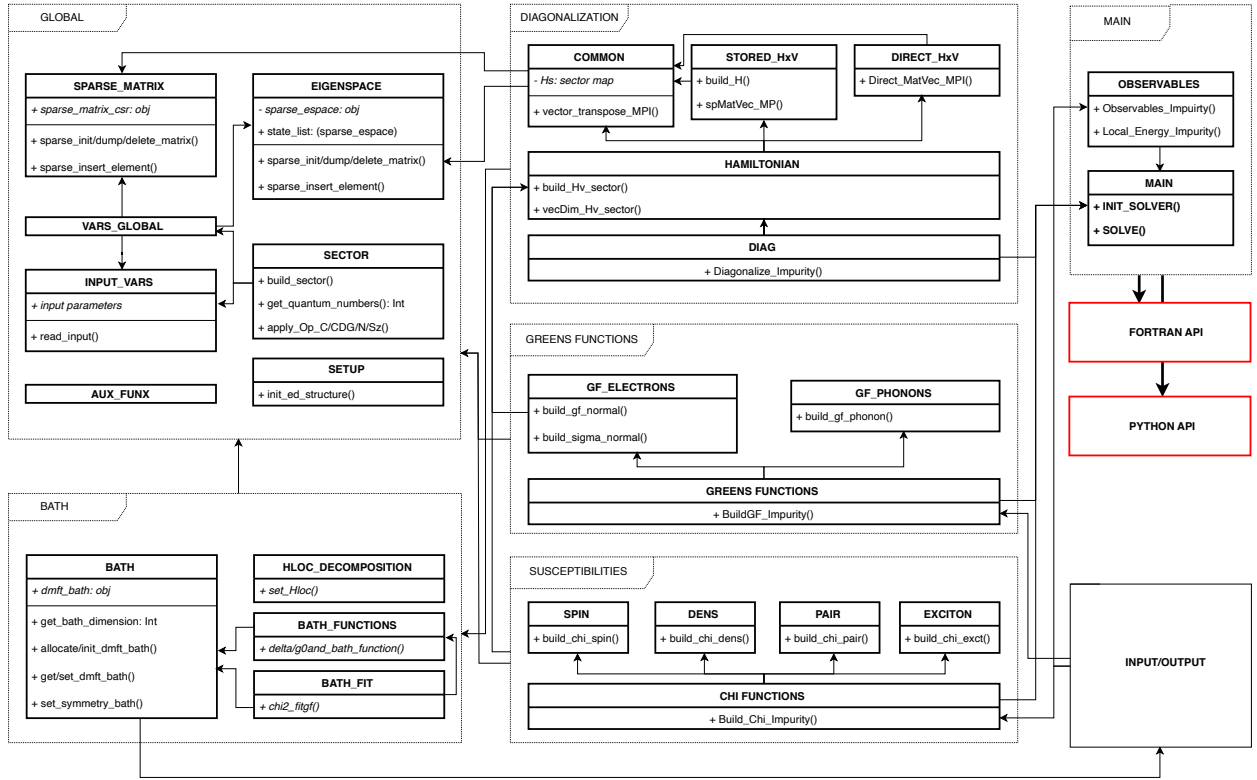


Figure 5: (Color online) Simplified UML diagram of the EDIpack library. The library is divided in several abstract work packages *Global*, *Bath*, *Diagonalization*, *GreensFunctions*, *Susceptibilities*, *Input/Output*, *Main* aimed to carry out specific tasks or to contain global objects or procedures. General classes and setup procedures are defined in the *Global* package. Discretized bath is handled in the *Bath* package. The hamiltonian matrix is diagonalized in the *Diagonalization* package and its results are used in *GreensFunctions*, *Susceptibilities* to construct dynamical correlations functions. The Fortran API, i.e. the library interfaces, is provided by the top end module EDIpack, providing access to a selected number of global procedures. The Python binding is built using the `numpy.f2py` tool on a Fortran layer in combination with a pure Python module.

ultimately making use of the Fortran intrinsic `move_alloc`. This ensures a faster execution compared to implicit reallocation, i.e. `vec=[vec,new_element]`. This solution enables to deal with the a priori unknown number of non-zero elements on each row, to optimize the memory footprint and to guarantee $O(1)$ access to any element of the matrix, which are crucial aspect to speed-up the execution of the MVP.

6.2. Eigenspace class

The storage of the eigenvalues and eigenvectors is a key aspect of the ED algorithm. In our implementation this task makes use of a dedicated class, defined in `EIGENSPACE`. The class contains the object `sparse_espac`: an ordered single linked list storing the eigenvalue (the sorting key), the eigenvector and the corresponding QNs. In parallel mode the eigenvectors are automatically distributed to all processors in shares of size `Q` (see Sec. 3) and can be accessed only through pointer functions to avoid memory duplication.

For zero temperature calculations only the ground-states are stored in the list. For a finite temperature also excited states are saved. In order to avoid unbounded growth of the list we adopt an annealing truncation mechanism. In the first call we collect a number `lanc_nstates_sector` of states from each sector, up to a given maximum number `lanc_nstates_total`, both initially set by the user. On the successive calls, the number of states required to any sector \mathcal{S} contributing to the list is increased by `lanc_nstates_step` or reduced otherwise. The total number of states with energy E stored in the list is fixed by the condition: $e^{-\beta(E-E_0)} < \text{cutoff}$, where E_0 is the groundstate energy, $\beta = 1/T$ is the inverse temperature ($k_B = 1$) and `cutoff` is an input parameter fixing an a priori energy threshold. An annealed list is constructed after few repeated calls, containing all and just the states contributing to the spectrum up to the required energy threshold.

6.3. Sector construction

The setup of the Fock space sectors is performed in the module `SECTOR`. The `build_sector` procedure is used to construct any given sector $\mathcal{S}[\vec{N}_\uparrow, \vec{N}_\downarrow]$ by setting up the map $\vec{\mathcal{M}}$. Operationally the map corresponds to a suitable structure which holds $2N_{ud}$ integer arrays. Any such array has a length $D_{\alpha\sigma}$, with $\alpha = 1, \dots, N_{ud}$, $\sigma = \uparrow, \downarrow$. The arrays are constructed iteratively by looping over the integers $I_{\alpha\sigma} = 0, \dots, 2^{N_{bit}} - 1$. The state index is appended into the array if its bit decomposition corresponds to the required QNs value. The key part of `build_sector` is shown below:

```

1  do iud=1,Ns_Ud
2    dim=0
3    do iup=0,2**Nbit-1
4      nup_ = popcnt(iup)
5      if(nup_ /= Nups(iud))cycle
6        dim = dim+1
7        H(iud)%map(dim) = iup
8    enddo
9    dim=0
10   do idw=0,2**Nbit-1
```

```

11     ndw_ = popcnt(idw)
12     if(ndw_ /= Ndws(iud)) cycle
13     dim = dim+1
14     H(iud+Ns_Ud)%map(dim) = idw
15     enddo
16 enddo

```

Inversion of such maps is achieved through a binary search reverse-lookup algorithm. The small performance loss in access time of order $O(N \log(N))$ is overly compensated by the lower memory footprint.

6.4. Bath class

Depending on the symmetries of the quantum impurity problem different topologies of the non-interacting bath can be devised. In the EDIpack library we include three general bath topologies. The three cases are selected by the input parameter `bath_type=normal, hybrid, replica`⁴⁵. In the first case (`normal`) N_b bath levels are coupled to each orbital, in the second the N_b bath levels couple to all the orbitals through different amplitudes. Finally, in the `replica` case, each bath level has the same local structure of the impurity site, with parameters to be determined, and couples to it via a single amplitude.

The bath is handled using a reverse communication strategy. Internally the bath is described by the class `dmft_bath`, defined in the module `BATH`. On the user side the bath parameters are stored in an single array of real numbers, which provides the main input of the solver. The correct dimensions of such array are retrieved using `get_bath_dimension` procedure.

6.5. Bath fit

In the DMFT context the bath is updated using a least square optimization. This is performed in the module `BATH_FIT` by means of a conjugate gradient minimization with respect to the parameters $\{V, h\}$ of the cost function:

$$\chi_\sigma = \sum_{n=1}^{N_{fit}} \frac{1}{W_n} \sum_{\alpha\beta} |X(i\omega_n) - X^{And}(i\omega_n; \{V, h\})|^q$$

where the parameter `cg_Scheme=Delta,Weiss` controls $X = \Delta, \mathcal{G}_0$, respectively, the hybridization function $\Delta(i\omega_n) = \sum_i V_i (i\omega_n - h^i)^{-1} V_i$ and the Weiss field $\mathcal{G}_0(i\omega_n) = [i\omega_n + \mu - H_{loc} - \Delta(i\omega_n)]^{-1}$. The fit weight $W_n = 1, 1/L_{fit}, 1/\omega_n$ is controlled by `cg_Weight`, the power q is controlled by `cg_pow` and the maximum number of frequencies L_{fit} is controlled by `Lfit` input variables. The gradient is evaluated either analytically or numerically as defined by the value of the input parameter `cg_grad`.

6.6. Local Hamiltonian

A crucial step in the setup of the impurity problem is the definition of the local non-interacting Hamiltonian term. This is performed by the procedure `set_Hloc` in the module

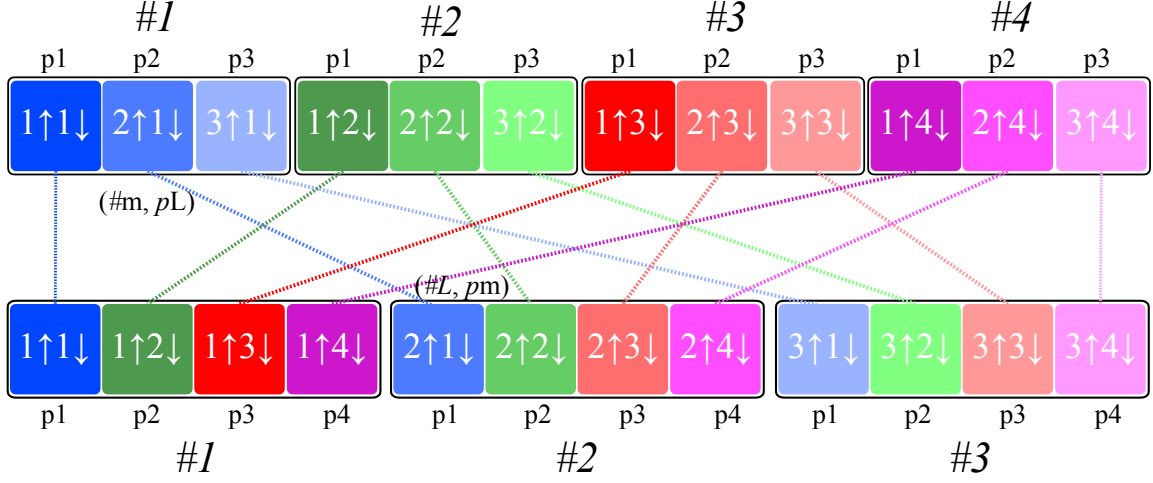


Figure 6: (Color online) Schematic representation of the `MPI.AllToAllV` parallel transposition of a vector. We consider the same case as in Fig. 1, i.e. vector dimensions $D_S = D_\uparrow \times D_\downarrow = 3 \times 4$ and $p=4$ processors. The initial vector (top part) is distributed so that each processor, indicated with $\#m$ and $m = 1, \dots, 4$, holds one column, corresponding to a different color. Each column contains 3 data components, indicated with pL , $L = 1, 2, 3$ and corresponding to different shades of the same color. Each vector component is identified by the pair $(\#m, pL)$. The procedure `MPI.AllToAllV` sends the element at L of the processor m to the processor L placing it at position m , i.e. each component $(\#m, pL)$ is moved to $(\#L, pm)$. The final result (bottom part) is the transposed vector. Note that processor 4 does not receive any component although it participates in the communication process.

HLOC_DECOMPOSITION. We envisage two methods to fix the local impurity Hamiltonian H_{loc} . The first is to pass directly the multi-dimensional array which represents such matrix. A second method, available for the `replica` bath, corresponds to consider the following matrix decomposition: $H_{loc} = \sum_{p=1}^{N_p} \lambda_p \Gamma_p$ in terms of a set of N_p variational parameters λ_p on the matrix basis Γ_p . A set of bath parameters λ_p is created for each bath level and optimized in the fit procedure outlined above.

6.7. Hamiltonian Matrix-Vector Product

The Hamiltonian matrix construction and the related MVPs operations are contained in the module `HAMILTONIAN`. Different type of MVP are envisaged depending on the input parameters `ed_Sparse_H` and `ed_total_ud` which, respectively, control the storage of the Hamiltonian and the type of QNs. In order to comply with the different operational modes the MVP is abstracted into a procedure contained in the global module `VARS_GLOBAL`:

```

1  abstract interface
2      subroutine dd_sparse_HxV(Q,v,Hv)
3          integer          :: Q
4          real(8),dimension(Q) :: v
5          real(8),dimension(Q) :: Hv
6      end subroutine dd_sparse_HxV

```

```

7   end interface
8   procedure(dd_sparse_HxV), pointer :: spHtimesV_p=>null()

```

The MPI setup, the Hamiltonian construction and the association of the pointer instance `spHtimesV_p` to the correct MVP procedure are performed in `build_Hv_sector`, contained in `HAMILTONIAN`. The matrix construction is performed in the module `HAMILTONIAN_SPARSE_HxV`. The sector Hamiltonian is represented by a hermitian matrix of dimension D_S^2 . The overall low connectivity of the quantum impurity models reflects in a strong sparseness of the Hamiltonian, which hosts at most $O(N_s) \ll D_S$ elements on each row. We exploit the Hamiltonian decomposition (9) to minimize the memory footprint storing each matrix component separately. The diagonal term H_d corresponds to a single vector of length D_S . The tensor product structure of the hopping terms can be readily reconstructed by storing the terms $H_{\alpha\sigma}$ in a tuple of sparse matrices,. The total dimension of such tuple is at most of order $O(N_{ud}N_s \max(D_{\alpha\sigma}))$, which is much smaller than $O(N_s D_S)$. Finally, H_{nd} is stored as a separate sparse matrix with a leading dimension D_S . This component has a very sparse nature, containing a number $n \ll N_s$ of elements per row.

The key part of the EDIpack library is the parallel execution of the MVPs using either the memory stored Hamiltonian or the on-the-fly execution. All the MVP instances are contained in the two modules `HAMILTONIAN_SPARSE_HxV` and `HAMILTONIAN_DIRECT_HxV`. As discussed above the fundamental step in the execution of each MVP is the parallel transposition of the incoming vector. The corresponding algorithm implementation is presented below:

```

1  subroutine vector_transpose_MPI(nrow,qcol,A,ncol,qrow,B)
2      integer  :: nrow,ncol,qrow,qcol
3      real(8)  :: A(nrow,qcol), B(ncol,qrow)
4      ...
5      counts = Nrow/MpiSize ; Ntot = Ncol/MpiSize ; if(mod(Ncol,MpiSize)/=0)Ntot=Ntot+1
6      do i=1,qcol
7          do irank=0,MpiSize-1
8              send_counts(irank,i) = counts
9              if(irank < mod(Nrow,MpiSize))send_counts(irank,i) = counts+1
10         enddo
11     enddo
12     do i=1,Ntot
13         call MPI_AllToAll(send_counts(0:,i),1,MPI_INTEGER,recv_counts(0:,i),1,&
14             MPI_INTEGER,MpiComm,ierr)
15     enddo
16     do i=1,Ntot
17         do irank=1,MpiSize-1
18             send_offset(irank,i) = send_counts(irank-1,i) + send_offset(irank-1,i)
19         enddo
20     enddo
21     recv_offset(0,1) = 0
22     do i=2,Ntot
23         recv_offset(0,i) = sum(recv_counts(0,:i-1))
24     enddo

```

```

25     do i=1,Ntot
26         do irank=1,MpiSize-1
27             recv_offset(irank,i) = recv_offset(irank-1,i) + sum(recv_counts(irank-1,:))
28         enddo
29     enddo
30     do j=1,Ntot
31         call MPI_AllToAllV(&
32             A(:,j),send_counts(:,j),send_offset(:,j),MPI_DOUBLE_PRECISION,&
33             B(:,j),recv_counts(:,j),recv_offset(:,j),MPI_DOUBLE_PRECISION,MpiComm,ierr)
34         enddo
35         call local_transpose(B,ncol,qrow)
36     end subroutine vector_transpose_MPI
37     subroutine local_transpose(mat,nrow,ncol)
38         integer                :: nrow,ncol
39         real(8),dimension(Nrow,Ncol) :: mat
40         mat = transpose(reshape(mat,[Ncol,Nrow]))
41     end subroutine local_transpose

```

The initial part of the procedure deals with the generic determination of the input arrays required by the `MPI_AllToAllV` procedure. In the first section (lines 5-11) the number of elements of the source buffer to be sent by each process is determined in the array `send_counts`. By construction, the corresponding amount of data received in the transposed buffer, i.e. `recv_counts`, is obtained by transposing the `send_counts` array itself using `MPI_AllToAll` (lines 12-14). Next, the relative displacements of the source and receive data with respect to their starting memory addresses, i.e. `send_offset` and `recv_offset`, are evaluated by summing over the number of elements to be sent/received, see lines 15-28. Finally, the matrix transposition is performed proceeding column-by-column, see lines 30-35. Note that some process may run out of columns to send because of the incommensurability of the matrix size with the number of processes. In this case MPI allows to send empty arrays. The final array is however arranged in row-major mode, thus a local transposition on each process is required to reorder the data in column-major mode.

Then, we present the implementation of the parallel MVP procedure, as described in Sec. 3.2:

```

1     ! MPI_MatVec(Q,v,Hv) - |Hv> = H_S|v>
2     subroutine spMatVec_mpi_main(Q,v,Hv)
3         integer                :: Q
4         real(8),dimension(Q),intent(in)  :: v
5         real(8),dimension(Q),intent(out) :: Hv
6         ...
7         !Local part: H_d|v>
8         Hv=0d0
9         do i=1,Q
10            do j=1,spH0d%row(i)%Size
11                Hv(i) = Hv(i) + spH0d%row(i)%vals(j)*v(i)
12            end do
13        end do
14        !Non-local part:

```

```

15  !↑-part  $H_{\uparrow}|v\rangle$  - contiguous in memory.
16  do idw=1,MpiQdw
17      do iup=1,DimUp
18          i = iup + (idw-1)*DimUp
19          hxv_up: do jj=1,spH0ups(1)%row(iup)%Size
20              jup = spH0ups(1)%row(iup)%cols(jj)
21              jdW = idw
22              val = spH0ups(1)%row(iup)%vals(jj)
23              j = jup + (idw-1)*DimUp
24              Hv(i) = Hv(i) + val*v(j)
25          end do hxv_up
26      enddo
27  end do
28  !↓-part  $H_{\downarrow}|v\rangle$  - non-contiguous in memory
29  mpiQup=DimUp/MpiSize ; if(MpiRank<mod(DimUp,MpiSize))MpiQup=MpiQup+1
30  allocate(vt(mpiQup*DimDw)) ;vt=0d0
31  allocate(Hvt(mpiQup*DimDw));Hvt=0d0
32  !MPI vector transposition  $|v\rangle \rightarrow |v\rangle^T = |vt\rangle$ 
33  call vector_transpose_MPI(DimUp,MpiQdw,v,DimDw,MpiQup,vt)
34  ! $|Hvt\rangle = H_{\downarrow}|vt\rangle$ 
35  Hvt=0d0
36  do idw=1,MpiQup          !<= Transposed order: column-wise DW <--> UP
37      do iup=1,DimDw      !<= Transposed order: column-wise DW <--> UP
38          i = iup + (idw-1)*DimDw
39          hxv_dw: do jj=1,spH0dws(1)%row(iup)%Size
40              jup = spH0dws(1)%row(iup)%cols(jj)
41              jdW = idw
42              j = jup + (jdW-1)*DimDw
43              val = spH0dws(1)%row(iup)%vals(jj)
44              Hvt(i) = Hvt(i) + val*vt(j)
45          end do hxv_dw
46      enddo
47  end do
48  deallocate(vt) ; allocate(vt(DimUp*mpiQdw)) ; vt=0d0
49  !Transpose back:  $|Hvt\rangle^T = |Hv\rangle$ 
50  call vector_transpose_MPI(DimDw,mpiQup,Hvt,DimUp,mpiQdw,vt)
51  Hv = Hv + Vt
52  deallocate(vt)
53  !Optional Non-Local terms:  $H_{nd}|v\rangle$ 
54  if(jhflag)then
55      N = 0 ; call AllReduce_MPI(MpiComm,Q,N)
56      allocate(vt(N)) ; vt = 0d0
57      !Reconstructs the vector gathering all CPUs shares, see SETUP
58      call allgather_vector_MPI(MpiComm,v,vt)
59      !Each process get its own share of the product
60      do i=1,Q
61          matmul: do j=1,spH0nd%row(i)%Size
62              Hv(i) = Hv(i) + spH0nd%row(i)%vals(j)*Vt(spH0nd%row(i)%cols(j))
63          enddo matmul
64      enddo
65      deallocate(Vt)

```

```
66     endif
67 end
```

6.8. Diagonalization

The Hamiltonian diagonalization and low-lying spectrum construction are performed in the module `DIAG`, using either P-Arpack^{43,44} or simple Lanczos procedure with no re-orthogonalization as controlled by the input variable `lanc_method=arpack,lanczos`. Sectors with dimensions smaller than the input value `lanc_dim_threshold` are diagonalized using Lapack method.

6.9. Observables

Local observables, such as occupation, double occupancies and local energy, are evaluated in the module `OBSERVABLES` using thermal average $\langle \mathcal{O} \rangle = \text{Tr} e^{-\beta H} \mathcal{O} / Z$. Having access to the lowest part of the spectrum we can evaluate the first terms in the thermodynamic trace: $\langle \mathcal{O} \rangle = \frac{1}{Z} \sum_n e^{-\beta E_n} \langle \psi_n | \mathcal{O} | \psi_n \rangle$, where $|\psi_n\rangle$ are the eigenstates of the system.

6.10. Dynamical correlation functions

The evaluation of the impurity Green's functions $G_{\alpha\beta}$ is executed in `GREENS_NORMAL` using the method outlined in Sec. 3.3. Similarly, spin, charge, excitonic and pair susceptibilities functions are evaluated in the modules `CHI_SPIN`, `CHI_DENS`, `CHI_EXCT` and `CHI_PAIR`. All the dynamical correlation functions are evaluated along the imaginary and real-frequency axis. The susceptibilities are also evaluated in imaginary time. The most time consuming part of this step is the construction of the Krylov basis $\mathcal{K}_N(\mathcal{O}|\psi_n)$ associated to each of the states $|\psi_n\rangle$ of the spectrum determined in the diagonalization step. This ultimately requires to perform a number N of MVP for any target state $|\psi_n\rangle$. The evaluation of a dynamical correlation function introduced an intrinsic small memory bottleneck, related to the non-local nature of the operator application $|\phi_n\rangle = \mathcal{O}|\psi_n\rangle$, which in our implementation is performed by the master node and subsequently distributed to the other processes.

7. Installation and usage

The EDIpack library is released under open source GNU GPL license. The source code is publicly available at the GitHub on-line repository: github.com/QcmPlab/EDIpack. For the installation few dependencies have to be satisfied. In particular the code relies on the open source scientific library SciFortran, available at github.com/QcmPlab/SciFortran:

- Fortran compiler with support to major fortran 90/2003 standard, e.g. GNU gfortran version > 9.0.0 or Intel ifort > 13.0.0.
- CMake > 3.0.0
- MPI
- SciFortran

Additional dependencies are required for the Python binding:

- Python, version >3.0.0
- Pkgconfig
- Numpy
- Mpi4py

7.1. Installation

The source code can be downloaded or cloned from the its official GitHub website. The build system is based on cmake. The loading into the operative system is achieved using either the provided shell script or the environment module. Should all the dependencies be satisfied and assuming to be in the main library directory, the compilation procedure is:

```
mkdir Build
cd Build
cmake .. [-DPREFIX=<${HOME}/opt/edipack/PLAT/VERSION>
         -DBUILD_TYPE=<RELEASE>/TESTING/DEBUG
         -DUSE_MPI=<yes>/no ]
make
make install
```

The Python binding can be installed once the library has been loaded in the system using either:

```
export F90=mpif90
pip install .
```

or

```
export F90=mpif90
python setup.py install
```

We tested installation of the EDIpack library in different platforms, e.g. common Linux distribution, Unix/OSX systems and dedicated HPC.

7.2. Basic usage

Two commented test codes are included in the `test` directory of the library. The codes solve the DMFT equations for the single band Hubbard model on the Bethe lattice, using either Fortran and Python API. The provided codes can be used as templates for other specific cases. A default input file is created as the program is executed in an empty directory. A list of the most important input variables are given in appendix. A *used* version of the input file, containing the variables actually used during the run, is written after each call to the main solver. The output of the library is controlled by several input variables. All the quantities evaluated within this package are written in multi-columns text files with appended suffix `.ed`. The naming convention is self-explanatory and, where necessary, header of multi-column files are automatically created.

Acknowledgements

We acknowledge fruitful discussions with G. Sangiovanni, A. Sartori, H. Choi, F. Petocchi, A. Valli, S. Adler and M. Chatzieftheriou. A.A. and M.C. acknowledge support from H2020 Framework Programme, under ERC Advanced Grant No. 692670 FIRSTORM and financial support from MIUR PRIN 2015 (Prot. 2015C5SEJJ001) and SISSA/CNR project “Superconductivity, Ferroelectricity and Magnetism in bad metals” (Prot. 232/2015). L.C. acknowledges financial support by the Deutsche Forschungsgemeinschaft (DFG, German Research Foundation) under Germany’s Excellence Strategy through Würzburg-Dresden Cluster of Excellence on Complexity and Topology in Quantum Matter - ct.qmat (EXC 2147, project-id 390858490). G.M. acknowledges support of the FNS/SNF through an Ambizione grant and partly supported from the European Research Council (ERC-319286-QMAC). L.d.M is supported by the European Commission through the ERC-CoG2016, StrongCoPhy4Energy, GA No 724177.

Appendix A: Input Variables

Here is reported a list of the most important global input variables of the library. The first column defines the name of the variables, the second their type and dimension `Type(Dim)` in Fortran standards. The last column provide a short description of the variable meaning.

<i>Variable</i>	<i>Description</i>
<code>Norb</code>	Number of impurity orbitals
<code>Nspin</code>	Number of spin channels treated independently. 1: non-magnetic, 2: magnetic
<code>Nbath</code>	Number of bath sites.
<code>Nloop</code>	Maximum number of allowed iterations in the DMFT solution
<code>Nph</code>	Maximum number of phonons
<code>Uloc</code>	Local intra-orbital interactions
<code>Ust</code>	Local inter-orbital interaction with opposite spin orientations
<code>Jh</code>	Hund’s coupling. This fixes the value of $U'' = U' - Jh$
<code>Jx</code>	Spin-Exchange coupling constant
<code>Jp</code>	Pair-Hopping coupling constant
<code>xmu</code>	Chemical potential. If <code>HFMODE=True</code> this value contains the Hartree shift, i.e. 0.0 sets the half-filling for a particle-hole symmetric case.
<code>beta</code>	Inverse temperature. At $T = 0$ this only sets a low-energy cut-off and discretization of Matsubara frequencies.

<i>Variable</i>	<i>Description</i>
<code>g_ph</code>	Electron-Phonon couplings
<code>w0_ph</code>	Phonon frequency
<code>eps</code>	Real-axis broadening
<code>wini, wfin</code>	Real-axis frequency range
<code>xmin, xmax</code>	Phonon probability distribution spatial range
<code>HFmode</code>	If True Hartree shift is included in the interaction
<code>cutoff</code>	Cutoff for the spectral summation, i.e. keep all states with energy E such that $e^{-\beta(E-E_0)} < \text{cutoff}$
<code>gs_threshold</code>	Energy threshold for the ground-state degeneracy.
<code>sb_field</code>	Small symmetry breaking field
<code>dmft_error</code>	Convergence threshold
<code>Nsuccess</code>	Minimum number of repeated iterations below threshold to reach convergence
<code>chispin_flag</code>	Flag to include the evaluation of Spin-Spin susceptibilities
<code>chidens_flag</code>	Flag to include the evaluation of Density-Density susceptibilities
<code>chipair_flag</code>	Flag to include the evaluation of Pair susceptibilities
<code>chiext_flag</code>	Flag to include the evaluation of Excitonic susceptibilities
<code>bath_type</code>	Set the bath type: <code>normal</code> : 1 bath level per orbital, <code>hybrid</code> : all bath levels shared, <code>replica</code> : bath levels are replicas of the impurity
<code>ed_finite_temp</code>	Flat to select finite temperature method. If True: <code>lanc_nstates_total > 1</code> is required
<code>ed_sparse_H</code>	Flag to select storage type of the sparse Hamiltonian. True: sparse matrix object, False: on-the-fly matrix-vector product
<code>ed_total_ud</code>	Flag to select quantum numbers type: True: total, False: orbital resolved
<code>ed_solve_offdiag_gf</code>	Flag to force the calculation of the off-diagonal Green's functions. True if <code>bath_type ≠ normal</code>
<code>ed_print_Sigma</code>	Flag to print out the impurity Self-energies
<code>ed_print_G</code>	Flag to print out the interacting impurity Green's functions
<code>ed_print_G0</code>	Flag to print out the non-interacting impurity Green's functions

<i>Variable</i>	<i>Description</i>
ed_all_G	Flag to evaluate all components of the impurity Green's functions, irrespective of the symmetries of the problem for <code>bath_type=replica</code>
ed_twin	Flag to reduce the number of visited sector using twin sectors symmetry: $[\vec{N}_\uparrow, \vec{N}_\downarrow] \leftrightarrow [\vec{N}_\downarrow, \vec{N}_\uparrow]$.
ed_verbose	Verbosity level [0-5]
lanc_method	String to select Lanczos method. <code>ARPACK</code> : uses P-Arpack, <code>LANCZOS</code> : uses single vector Lanczos method with no reorthogonalization
lanc_tolerance	Tolerance for the Lanczos iterations
lanc_niter	Largest number of Lanczos iterations for spectrum analysis
lanc_ngfiter	Largest dimension of the Krylov basis in the evaluation of the Green's function
lanc_ncv_factor	Factor to determine block size <code>Ncv</code> used in P-Arpack as by (<code>Ncv = lanc_ncv_factor * Neigen + lanc_ncv_add</code>)
lanc_ncv_add	Factor to determine block size <code>Ncv</code> used in P-Arpack as by (<code>Ncv = lanc_ncv_factor * Neigen + lanc_ncv_add</code>)
lanc_nstates_sector	Maximum number of eigenvalues per sector required to P-Arpack. For $T > 0$ this number is adjusted during annealing
lanc_nstates_total	Maximum number of states in the spectrum retained for $T > 0$. See <code>cutoff</code>
lanc_nstates_step	Number of states added to <code>lanc_nstates_sector</code> during annealing
lanc_dim_threshold	Dimension threshold above which Lanczos method is used to determine spectrum states
cg_Scheme	Conjugate Gradient fit scheme. <code>Delta</code> : fit $\Delta(i\omega_n)$, <code>Weiss</code> : fit $\mathcal{G}_0(i\omega_n)$
cg_method	Conjugate Gradient fit method. 0:Fletcher-Reeves-Polak-Ribiere minimisation, 1:unknown f77 minimize subroutine
cg_grad	Type of gradient evaluation. 0: Analytic, 1: Numeric
cg_Niter	Maximum number of iteration in the Conjugate Gradient fit
cg_Ftol	Tolerance in the Conjugate Gradient fit
cg_stop	Stop condition for the Conjugate Gradient fit. 0: $C_1 + C_2$, 1: C_1 , 2: C_2 with $C_1 = F_{n-1} - F_n < \text{cg_Ftol} * (1 + F_n)$, $C_2 = \ x_{n-1} - x_n\ < \text{cg_Ftol} * (1 + \ x_n\)$
cg_Weight	Conjugate Gradient fit weight. 0: 1, 1: $1/\text{Lfit}$, 2: $1/\omega_n$

<i>Variable</i>	<i>Description</i>
<code>cg_pow</code>	fConjugate Gradient fit exponent as $ \mathcal{G}_0 - \mathcal{G}_0^{And} _{\text{cg_pow}}$
<code>Lmats</code>	Number of Matsubara frequencies
<code>Lreal</code>	Number of real-axis frequencies
<code>Lfit</code>	Number of Matsubara frequencies for the Conjugate Gradient fit. $Lfit \leq Lmats$
<code>Hfile</code>	File name to read/write bath parameters
<code>LOGfile</code>	Fortran Unit [6:999] for execution log output

Appendix B: Main procedures

Here is a list of the fundamental procedures accessible from this library. Some procedures have both serial and parallel behavior. The latter can be accessed passing the MPI communicator `MpiComm` as input. The inputs in square brackets are optional.

<i>PROCEDURE</i>	<i>INFO</i>
<code>ed_read_input(File, [MpiComm])</code>	Read global input variables from <code>File</code> .
<code>ed_set_Hloc(Hloc/Hvec, LambdaVec)</code>	Set the local part of the non-interacting Hamiltonian determining the impurity, see Sec. 6.6. The input is either in the form of an array <code>Hloc [Nspin, Nspin, Norb, Norb]</code> or a couple <code>Hvec = Γ [Nspin, Npin, Norb, Norb, N_p]</code> , <code>Lambdavec = λ [N_p]</code>
<code>ed_get_bath_dimension([Hloc])</code>	Retrieve the correct dimension <code>Nb</code> of the array <code>Bathh [Nb, [Nsites]]</code> storing the bath parameters. This value depends on <code>Norb</code> , <code>Nbath</code> and <code>bath_type</code> input variables
<code>ed_init_solver([MpiComm], Bath, [Hloc])</code>	Initialize the whole calculation, allocate the memory and prepare global variables. On input the <code>Bath</code> array is empty. On output <code>Bath</code> is either guessed or read from file. This procedure must be called before <code>ed_solve</code>
<code>ed_solve([MpiComm], Bath, [Hloc])</code>	Solve the impurity problem for a given <code>Bath</code> array
<code>ed_chi2_fitgf([MpiComm], Func, Bath, Hloc)</code>	Fit a local function <code>Func</code> using Conjugate Gradient to update the bath <code>Bath</code>

<i>PROCEDURE</i>	<i>INFO</i>
<code>ed_get_sigma_matsubara(Func, [Nsites])</code>	Returns the Matsubara self-energy function in <code>Func</code>
<code>ed_get_sigma_realaxis(Func, [Nsites])</code>	Returns the real-axis self-energy function in <code>Func</code>
<code>ed_get_gimp_matsubara(Func, [Nsites])</code>	Returns the Matsubara impurity Green's function in <code>Func</code>
<code>ed_get_gimp_realaxis(Func, [Nsites])</code>	Returns the real-axis impurity Green's function in <code>Func</code>
<code>ed_get_dens(Var, [Nsites])</code>	Returns the impurity occupations in <code>Var</code>
<code>ed_get_mag(Var, [Nsites])</code>	Returns the impurity magnetization in <code>Var</code>
<code>ed_get_docc(Var, [Nsites])</code>	Returns the impurity double occupancy in <code>Var</code>
<code>ed_spin_symmetrize_bath(Bath)</code>	Enforce spin symmetry in the bath <code>Bath</code>
<code>ed_break_symmetry_bath(Bath, Field, Sign)</code>	Breaks spin symmetry in the bath <code>Bath</code> using a small field of amplitude <code>Field</code> and sign <code>Sign</code>

References

References

- [1] H. Lin, J. Gubernatis, [Exact diagonalization methods for quantum systems](#), Computers in Physics 7 (4) (1993) 400–407.
URL <https://doi.org/10.1063/1.4823192>
- [2] A. C. Hewson, The Kondo Problem to Heavy Fermions, Cambridge University Press, New York, N.Y., 1993.
- [3] G. Kotliar, D. Vollhardt, [Strongly correlated materials: Insights from dynamical mean-field theory](#), Physics Today 57 (3) (2004) 53–59.
URL <https://doi.org/10.1063/1.1712502>
- [4] A. Georges, G. Kotliar, W. Krauth, M. J. Rozenberg, [Dynamical mean-field theory of strongly correlated fermion systems and the limit of infinite dimensions](#), Rev. Mod. Phys. 68 (1996) 13–125.
[doi:10.1103/RevModPhys.68.13](https://doi.org/10.1103/RevModPhys.68.13)
URL <https://link.aps.org/doi/10.1103/RevModPhys.68.13>
- [5] A. Georges, [Strongly correlated electron materials: Dynamical mean-field theory and electronic structure](#), AIP Conference Proceedings 715 (1) (2004) 3–74. [doi:10.1063/1.1800733](https://doi.org/10.1063/1.1800733).
URL <https://aip.scitation.org/doi/abs/10.1063/1.1800733>
- [6] F. Lechermann, A. Georges, A. Poteryaev, S. Biermann, M. Posternak, A. Yamasaki, O. K. Andersen, [Dynamical mean-field theory using Wannier functions: A flexible route to electronic structure calculations of strongly correlated materials](#), Phys. Rev. B 74 (12) (2006) 125120. [doi:10.1103/PhysRevB.74.125120](https://doi.org/10.1103/PhysRevB.74.125120).
URL <http://link.aps.org/abstract/PRB/v74/e125120>
- [7] M. Potthoff, [Self-energy-functional approach to systems of correlated electrons](#), The European Physical Journal B - Condensed Matter and Complex Systems 32 (4) (2003) 429–436. [doi:10.1140/epjb/](https://doi.org/10.1140/epjb/)

- e2003-00121-8.
 URL <https://doi.org/10.1140/epjb/e2003-00121-8>
- [8] D. Sénéchal, The variational cluster approximation for hubbard models: Practical implementation, in: 2008 22nd International Symposium on High Performance Computing Systems and Applications, 2008, pp. 9–15.
- [9] M. Potthoff, [Static and dynamic variational principles for strongly correlated electron systems](#), AIP Conference Proceedings 1419 (1) (2011) 199–258. doi:10.1063/1.3667325.
 URL <https://aip.scitation.org/doi/abs/10.1063/1.3667325>
- [10] M. Nuss, E. Arrigoni, M. Aichhorn, W. von der Linden, Variational cluster approach to the single impurity anderson model (2011). [arXiv:1110.4533](#).
- [11] B. Bauer, L. D. Carr, H. G. Evertz, A. Feiguin, J. Freire, S. Fuchs, L. Gamper, J. Gukelberger, E. Gull, S. Guertler, A. Hehn, R. Igarashi, S. V. Isakov, D. Koop, P. N. Ma, P. Mates, H. Matsuo, O. Parcollet, G. Pawłowski, J. D. Picon, L. Pollet, E. Santos, V. W. Scarola, U. Schollwöck, C. Silva, B. Surer, S. Todo, S. Trebst, M. Troyer, M. L. Wall, P. Werner, S. Wessel, [The ALPS project release 2.0: open source software for strongly correlated systems](#), Journal of Statistical Mechanics: Theory and Experiment 2011 (05) (2011) P05001. doi:10.1088/1742-5468/2011/05/p05001.
 URL <https://doi.org/10.1088/1742-5468/2011/05/p05001>
- [12] O. Parcollet, M. Ferrero, T. Ayrál, H. Hafermann, I. Krivenko, L. Messio, P. Seth, [Triqs: A toolbox for research on interacting quantum systems](#), Computer Physics Communications 196 (2015) 398–415. doi:https://doi.org/10.1016/j.cpc.2015.04.023.
 URL <https://www.sciencedirect.com/science/article/pii/S0010465515001666>
- [13] E. Gull, A. J. Millis, A. I. Lichtenstein, A. N. Rubtsov, M. Troyer, P. Werner, [Continuous-time monte carlo methods for quantum impurity models](#), Rev. Mod. Phys. 83 (2011) 349–404. doi:10.1103/RevModPhys.83.349.
 URL <https://link.aps.org/doi/10.1103/RevModPhys.83.349>
- [14] A. N. Rubtsov, V. V. Savkin, A. I. Lichtenstein, [Continuous-time quantum monte carlo method for fermions](#), Phys. Rev. B 72 (2005) 035122. doi:10.1103/PhysRevB.72.035122.
 URL <https://link.aps.org/doi/10.1103/PhysRevB.72.035122>
- [15] K. Haule, [Quantum monte carlo impurity solver for cluster dynamical mean-field theory and electronic structure calculations with adjustable cluster base](#), Phys. Rev. B 75 (15) (2007) 155113. doi:10.1103/PhysRevB.75.155113.
 URL <http://link.aps.org/abstract/PRB/v75/e155113>
- [16] P. Seth, I. Krivenko, M. Ferrero, O. Parcollet, [Triqs/cthyb: A continuous-time quantum monte carlo hybridisation expansion solver for quantum impurity problems](#), Computer Physics Communications 200 (2016) 274–284. doi:https://doi.org/10.1016/j.cpc.2015.10.023.
 URL <https://www.sciencedirect.com/science/article/pii/S001046551500404X>
- [17] M. Wallerberger, A. Hausoel, P. Gunacker, A. Kowalski, N. Parragh, F. Goth, K. Held, G. Sangiovanni, [w2dynamics: Local one- and two-particle quantities from dynamical mean field theory](#), Computer Physics Communications 235 (2019) 388–399. doi:https://doi.org/10.1016/j.cpc.2018.09.007.
 URL <https://www.sciencedirect.com/science/article/pii/S0010465518303217>
- [18] R. Žitko, T. Pruschke, [Energy resolution and discretization artifacts in the numerical renormalization group](#), Phys. Rev. B 79 (2009) 085106. doi:10.1103/PhysRevB.79.085106.
 URL <https://link.aps.org/doi/10.1103/PhysRevB.79.085106>
- [19] R. Bulla, T. A. Costi, D. Vollhardt, Finite-temperature numerical renormalization group study of the Mott transition, Phys. Rev. B 64 (4) (2001) 045103. doi:10.1103/PhysRevB.64.045103.
- [20] R. Bulla, T. A. Costi, T. Pruschke, [Numerical renormalization group method for quantum impurity systems](#), Rev. Mod. Phys. 80 (2) (2008) 395. doi:10.1103/RevModPhys.80.395.
 URL <http://link.aps.org/abstract/RMP/v80/p395>
- [21] S. R. White, Density matrix formulation for quantum renormalization groups, Phys. Rev. Lett. 69 (19) (1992) 2863–2866. doi:10.1103/PhysRevLett.69.2863.
- [22] K. A. Hallberg, Density-matrix algorithm for the calculation of dynamical properties of low-dimensional

- systems, Phys. Rev. B 52 (14) (1995) R9827–R9830. doi:10.1103/PhysRevB.52.R9827.
- [23] D. J. García, K. Hallberg, M. J. Rozenberg, Dynamical mean field theory with the density matrix renormalization group, Phys. Rev. Lett. 93 (2004) 246403. doi:10.1103/PhysRevLett.93.246403. URL <https://link.aps.org/doi/10.1103/PhysRevLett.93.246403>
- [24] U. Schollwöck, The density-matrix renormalization group, Rev. Mod. Phys. 77 (1) (2005) 259. doi:10.1103/RevModPhys.77.259. URL <http://link.aps.org/abstract/RMP/v77/p259>
- [25] F. A. Wolf, A. Go, I. P. McCulloch, A. J. Millis, U. Schollwöck, Imaginary-time matrix product state impurity solver for dynamical mean-field theory, Phys. Rev. X 5 (2015) 041032. doi:10.1103/PhysRevX.5.041032. URL <https://link.aps.org/doi/10.1103/PhysRevX.5.041032>
- [26] M. Caffarel, W. Krauth, Exact diagonalization approach to correlated fermions in infinite dimensions: Mott transition and superconductivity, Phys. Rev. Lett. 72 (1994) 1545–1548. doi:10.1103/PhysRevLett.72.1545. URL <https://link.aps.org/doi/10.1103/PhysRevLett.72.1545>
- [27] A. Dolfen, Massively parallel exact diagonalization of strongly correlated systems, Master’s thesis, Forschungszentrum Juelich (2006). URL <https://www.fz-juelich.de/cae/servlet/contentblob/1040316/publicationFile/23068/Dolfen.pdf>
- [28] C. A. Perroni, H. Ishida, A. Liebsch, Exact diagonalization dynamical mean-field theory for multiband materials: Effect of coulomb correlations on the fermi surface of $\text{na}_{0.3}\text{coo}_2$, Phys. Rev. B 75 (2007) 045125. doi:10.1103/PhysRevB.75.045125. URL <https://link.aps.org/doi/10.1103/PhysRevB.75.045125>
- [29] M. Capone, L. de’ Medici, A. Georges, Solving the dynamical mean-field theory at very low temperatures using the lanczos exact diagonalization, Phys. Rev. B 76 (2007) 245116. doi:10.1103/PhysRevB.76.245116. URL <https://link.aps.org/doi/10.1103/PhysRevB.76.245116>
- [30] C. Weber, A. Amaricci, M. Capone, P. B. Littlewood, Augmented hybrid exact-diagonalization solver for dynamical mean field theory, Phys. Rev. B 86 (2012) 115136. doi:10.1103/PhysRevB.86.115136. URL <http://link.aps.org/doi/10.1103/PhysRevB.86.115136>
- [31] Y. Lu, M. W. Haverkort, Exact diagonalization as an impurity solver in dynamical mean field theory, The European Physical Journal Special Topics 226 (11) (2017) 2549–2564. doi:10.1140/epjst/e2017-70042-4. URL <https://doi.org/10.1140/epjst/e2017-70042-4>
- [32] A. Weiße, H. Fehske, Exact Diagonalization Techniques, Springer Berlin Heidelberg, Berlin, Heidelberg, 2008, pp. 529–544. doi:10.1007/978-3-540-74686-7_{_}18. URL https://doi.org/10.1007/978-3-540-74686-7_18
- [33] A. W. Sandvik, Computational studies of quantum spin systems, AIP Conference Proceedings 1297 (1) (2010) 135–338. arXiv:<https://aip.scitation.org/doi/pdf/10.1063/1.3518900>, doi:10.1063/1.3518900. URL <https://aip.scitation.org/doi/abs/10.1063/1.3518900>
- [34] T. Siro, A. Harju, Exact diagonalization of the hubbard model on graphics processing units, Computer Physics Communications 183 (9) (2012) 1884–1889. doi:<https://doi.org/10.1016/j.cpc.2012.04.006>. URL <https://www.sciencedirect.com/science/article/pii/S0010465512001452>
- [35] U. Borštnik, J. VandeVondele, V. Weber, J. Hutter, Sparse matrix multiplication: The distributed block-compressed sparse row library, Parallel Computing 40 (5) (2014) 47–58. doi:<https://doi.org/10.1016/j.parco.2014.03.012>. URL <https://www.sciencedirect.com/science/article/pii/S0167819114000428>
- [36] T. Siro, A. Harju, Exact diagonalization of quantum lattice models on coprocessors, Computer Physics Communications 207 (2016) 274–281. doi:<https://doi.org/10.1016/j.cpc.2016.07.018>.

- URL <https://www.sciencedirect.com/science/article/pii/S0010465516302065>
- [37] M. Sharma, M. Ahsan, **Organization of the hilbert space for exact diagonalization of hubbard model**, *Computer Physics Communications* 193 (2015) 19–29. doi:<https://doi.org/10.1016/j.cpc.2015.03.014>.
URL <https://www.sciencedirect.com/science/article/pii/S0010465515001137>
- [38] C. Lanczos, **An iteration method for the solution of the eigenvalue problem of linear differential and integral operators**, *J. Res. Natl. Bur. Stand. B* 45 (1950) 255–282. doi:[10.6028/jres.045.026](https://doi.org/10.6028/jres.045.026).
- [39] W. E. ARNOLDI, **The principle of minimized iterations in the solution of the matrix eigenvalue problem**, *Quarterly of Applied Mathematics* 9 (1) (1951) 17–29.
URL <http://www.jstor.org/stable/43633863>
- [40] A. Krylov, **De la résolution numérique de l'équation servant à déterminer dans des questions de mécanique appliquée les fréquences de petites oscillations des systèmes matériels**, *Bulletin de l'Académie des Sciences de l'URSS* (5) (1931) 491–539.
URL <http://mi.mathnet.ru/izv5215>
- [41] E. Polizzi, **Density-matrix-based algorithm for solving eigenvalue problems**, *Phys. Rev. B* 79 (2009) 115112. doi:[10.1103/PhysRevB.79.115112](https://doi.org/10.1103/PhysRevB.79.115112).
URL <https://link.aps.org/doi/10.1103/PhysRevB.79.115112>
- [42] A. Georges, L. de' Medici, J. Mravlje, **Strong Correlations from Hund's Coupling.**, *Annu. Rev. Condens. Matter Phys.* 45 (2013) 137–178.
- [43] R. Lehoucq, D. Sorensen, C. Yang, **ARPACK Users' Guide: Solution of Large-scale Eigenvalue Problems with Implicitly Restarted Arnoldi Methods**, *Software, Environments, Tools, Society for Industrial and Applied Mathematics*, 1998.
URL https://books.google.it/books?id=iMUea23N_CQC
- [44] K. J. Maschhoff, D. C. Sorensen, **P_arpac: An efficient portable large scale eigenvalue package for distributed memory parallel architectures**, in: J. Waśniewski, J. Dongarra, K. Madsen, D. Olesen (Eds.), *Applied Parallel Computing Industrial Computation and Optimization*, Springer Berlin Heidelberg, Berlin, Heidelberg, 1996, pp. 478–486.
- [45] E. Koch, G. Sangiovanni, O. Gunnarsson, **Sum rules and bath parametrization for quantum cluster theories**, *Phys. Rev. B* 78 (2008) 115102. doi:[10.1103/PhysRevB.78.115102](https://doi.org/10.1103/PhysRevB.78.115102).
URL <https://link.aps.org/doi/10.1103/PhysRevB.78.115102>